Miguel Fernandes Duarte
Licenciado em Ciências de Engenharia Biomédica

Causal characterization of functional connectivity through the spread of electrically induced oscillations in the epileptic human brain

Dissertação para a obtenção do Grau de Mestre em
Engenharia Biomédica

Orientador: Antoni Valéro-Cabré, MD PhD,
Institut du Cérveau et de la Moèlle Épinière

Co-orientador: Julià L. Amengual, PhD,
Institut du Cérveau et de la Moèlle Épinière

Co-orientador: Carla Quintão, PhD,
Faculdade de Ciências e Tecnologias da Universidade Nova de Lisboa

Júri:

Presidente: José Luís Ferreira, PhD,
Faculdade de Ciências e Tecnologias da Universidade Nova de Lisboa

Arguente: Ricardo Vigário, PhD,
Faculdade de Ciências e Tecnologias da Universidade Nova de Lisboa

Vogal: Carla Quintão, PhD,
Faculdade de Ciências e Tecnologias da Universidade Nova de Lisboa

Setembro, 2017

FACULDADE DE
CIÊNCIAS E TECNOLOGIA
UNIVERSIDADE NOVA DE LISBOA

Miguel Fernandes Duarte
Licenciado em Ciências de Engenharia Biomédica

Causal characterization of functional connectivity through the spread of electrically induced oscillations in the epileptic human brain

Dissertação para a obtenção do Grau de Mestre em
Engenharia Biomédica

Orientador: Antoni Valéro-Cabré, MD PhD,
Institut du Cérveau et de la Moèlle Épinière

Co-orientador: Julià L. Amengual, PhD,
Institut du Cérveau et de la Moèlle Épinière

Co-orientador: Carla Quintão, PhD,
Faculdade de Ciências e Tecnologias da Universidade Nova de Lisboa

Setembro, 2017

Causal characterization of functional connectivity through the spread of electrically induced oscillations in the epileptic human brain

Acknowledgements

This thesis would not be complete without the help of so many. To those at the Institut du Cérveau et de la Moélle Épinière (ICM) and specifically at the FrontLab, thank you for making me feel at ease and at home on the five months I spent there. In what regards the people of the ICM, I have to especially pay compliments to both my supervisors, Antoni Valéro-Cabré and Julià Améngual (whose baby made his work even tougher), who made everything in their reach to make this project as best as it could have been. I have also to thank the people from Université Paris Descartes and from the Bioengineering and Inovation in Neurosciences track at the Master in Biomedical Engineering in Paris, that taught me a lot during my stay.

To my friends at the Maison du Portugal, in Paris, whose help was essential in this period I was abroad, particularly from those that did eat a lot of Ramen. It's food for thought. Without them, living in Paris would have been less beautiful, less fun, more sad.

To my good friends I made while studying at FCT-UNL (Alheiras, you know who I'm talking to), I can't thank you enough for these whole five years we have all been through while completing this Master. Those years can't be taken back and will always stay in my mind.

To my parents, my brother and my grandmother, whose preocupation and pledge for effort made me want to finish this Master in the best possible manner.

Of course I couldn't end this without thanking Beatriz Gaspar, my girlfriend who has been with me for most of this period, that has helped me when I felt I couldn't do it, that was here whenever she was needed, even while we were living countries apart. This thesis is also yours.

Abstract

Little is known about the rules governing the spread of local entrainment within synchronized networks distributed across the brain. The assessment of the causal influences impacting information flow between two brain regions have mainly relied on confirmatory model-driven approaches (such as dynamic causal modeling and structural equation modeling) and exploratory data driven approaches (such as Granger Causality analysis). However, stimulation-driven approaches offer a unique opportunity to impact ongoing brain activity and describe the causal consequences of such manipulations, performed on a specific node of a complex cerebral network.

In this project, we characterize causal functional interactions between brain regions by assessing how frequency-tuned electrical currents delivered intracranially in awaken epileptic patients enhance inter-regional synchrony between pairs of areas.

To achieve this goal, we worked with an existing iEEG database from 18 medication-resistant epilepsy patients undergoing Intracortical Stimulation Mapping Procedures (ISMP) performed to causally identify and localize the epileptogenic foci, prior to neurosurgical removal. Patients are implanted with series of multi-electrodes in well-known brain regions under MRI guidance.

Intracranial EEG contacts allow continuous recordings and the delivery through pairs of adjacent contacts of biphasic pulses of rhythmic Direct Electric Stimulations (DES) at a 50Hz frequency coupled to electrophysiological recordings.

Measuring significant increases in gamma power (50Hz) observed during the stimulation period (vs. prior the stimulation), and significant increases of Phase-Locking Value (PLV) between signals recorded in the electrically stimulated regions and activity evoked in the rest of implanted regions during stimulation (vs. prior simulation), we characterize the spread of oscillatory entrainment from the stimulated region to the remaining regions, thus establishing a network of functional connectivity in the brain. By comparing this network with the one shown during resting-state, we assess how entrainment to frequency-tuned electrical currents delivered intracranially is predicted by the resting-state functional connectivity network.

Keywords: Brain, Connectivity, Epilepsy, Stimulation, iEEG

Resumo

Pouco é conhecido acerca das regras que governam a propagação de arrastamento (*entrainment*) local em redes sincronizadas distribuídas ao longo do cérebro. A avaliação das influencias causais que influenciam o fluxo de informação entre duas regiões cerebrais tem maioritariamente dependido em abordagens confirmatórias usando modelos (como *dynamical causal modeling* e *structural equation modeling*) ou através de abordagens de exploração de dados (como análises da causalidade de Granger). No entanto, as abordagens através de estimulação oferecem a oportunidade única de influenciar a actividade cerebral em andamento e de descrever as consequências causais dessas manipulações, feitas em nós específicos de uma complexa rede cerebral.

Neste projecto, caracterizamos as interacções funcionais causais entre regiões cerebrais, avaliando como a sincronia inter-regional entre pares de regiões cerebrais é modificada quando sujeitas a correntes eléctricas de 50Hz, administradas intracranianamente em pacientes epilépticos acordados.

Utilizámos uma já existente base-de-dados de iEEG adquirida em 18 pacientes epilépticos resistentes à medicação, quando estes foram submetidos a estimulações intracorticais para, causalmente, identificar e localizar o foco epileptogénico, de modo a ser retirado. Para tal, os pacientes são implantados com séries de multi-eléctrodos em regiões cerebrais identificadas e determinadas clinicamente.

Os contactos do EEG intracranial permitem a gravação contínua e a libertação, através de pares de contactos adjacentes, de rítmicos pulsos bifásicos de Estimulação Eléctrica Directa (EED), a uma frequência de 50Hz.

Medindo aumentos significativos de potência gama (50Hz) observadas durante o período de estimulação (vs. antes da estimulação), e aumentos significativos de *Phase-Locking Value*, caracterizamos a propagação do arrastamento oscilatório da região estimulada para as restantes. Assim, estabelecemos uma rede de conectividade cerebral no cérebro. Ao comparar esta rede com a manifestada durante o estado de repouso, avaliamos de que forma o arrastamento a correntes eléctricas de 50Hz libertadas intracranialmente é previsto pela rede de conectividade funcional em estado de repouso.

Palavras-Chave: Cérebro, Conectividade, Epilépsia, Estimulação, iEEG

Contents

List of Figures

Page

List of Tables

Page

Chapter 1

Introduction and State of the Art

The human brain remains the object of a long set of unanswered questions inquiring on how this organ operates and behaves. For more than a century, influenced by the notion of neural systems conceived as highly specialized local systems (each underlying specific cognitive operations), brain research focused in the study of local systems and interactions. Nonetheless, relatively recent work strongly suggests that the human brain integrates sets of local networks that build up onto more complex highly interconnected global systems, making "the one more than just the sum of its parts".

Indeed, considering the brain as a modularly organized highly integrated system, brain connectivity has risen to become a highly influent topic, instrumental for the advancement of brain sciences and the treatment of its diseases and conditions.

One of the main emerging properties of neural systems and their connectivity is the ability to produce rhythmic patterns of activity. In continuity with the local vs. widespread conception of neural systems mentioned above, correlational evidence in humans suggests that high-level cognitive function strongly relays on coherent fluctuations of oscillatory patterns along widely synchronized brain networks. In these settings, neural rhythms are generated by the synchronized activation of local and/or widespread networks of neuronal populations, which have proven key to generate the coding mechanisms allowing flexible and efficient inter-regional communication, subtending cognition and ultimately leading to human behaviour.

Unfortunately, the relation between local and widespread structural and functional networks with behaviour has been often addressed through correlational measures, such as resting state or task activated Electroencephalography (EEG), Magnetoencephalography (MEG) or functional Magnetic Resonance Imaging (fMRI) which are prone to epiphenomena, i.e., they often incur in the risk to consider as causally related, tasks- or state-irrelevant patterns of activity generated in specific brain locations (or across networks) as causally related to a given function, when they only happen to coincide in time and space.

Particularly, since the advent, 20 years ago, of non-invasive focal brain stimulation methods, such as Transcranial Magnetic Stimulation (TMS), the notion that those reliably probing causal brain-behaviour relationships require the use of perturbation approaches, has been growing. This so called causal or ¨perturbation approach prones that, to better understand how neural structure generates function, it is paramount to probe if and in which way neural electrical coding (and if possible also associated cognition and behaviours) are altered when the brain is subjected to electrical discharges and map the distribution of activity across anatomical systems.

Along the lines of what lesion studies have been doing for more than a century, Transcranial Magnetic Stimulation (TMS), based on the use of high intensity shot lasting magnetic pulses applied to the scalp, has been able to induce focal electrical currents in the brain gray matter. Used in isolation or combined with EEG, TMS has been instrumental to provide causal or perturbation-based evidence of brain-behavioural relations in humans. Unfortunately, the often insufficient focality (1.5-2 cm diameter), uncertain mechanism of activation (mediated by local intracortical interneurons), the poor spatial resolution and difficulties for adequate source localisation of evoked changes in EEG signals, call for complementary approaches to tackle such a fundamental question. In this context, we turned to intracranial EEG recordings performed in human epileptic patients in isolation or combined with bursts of singe pulse (1 Hz) and 50 Hz direct brain intracranial stimulation for pre-surgical mapping purposes. At the expense of

the potential influence of a brain condition such as epilepsy on normal cerebral excitability and coding dynamics, and biases in brain sampled regions, often focalized in temporal regions, intracranial stimulation perturbation approaches have the potential to overcome the above-stated focality limitations and uncertainties, if one can cumulate data from a sufficiently large cohort of cases. Hence, we aim to compile and compare qualitatively functional connectivity patterns of the human brain on the basis of intracranial direct brain recordings at resting-state or during the delivery of 50 Hz direct intracranial stimulation.

1.1 Connectivity and Causality

Connectivity deals with the way in which activity patterns recorded in pairs of regions or sites are temporally related and how they interact dynamically over space and time. The conjunction of pair-wise connectivity interactions between all possible combinations of sampled sites can be combined to define a connectome. In the human brain, sites correspond to the different discreet brain regions from which recording can be focally measured. Three different subtypes of brain connectivity have been thus far defined (see Figure 1.1): *Structural connectivity, Functional connectivity* and *Effective connectivity*[3, 4].

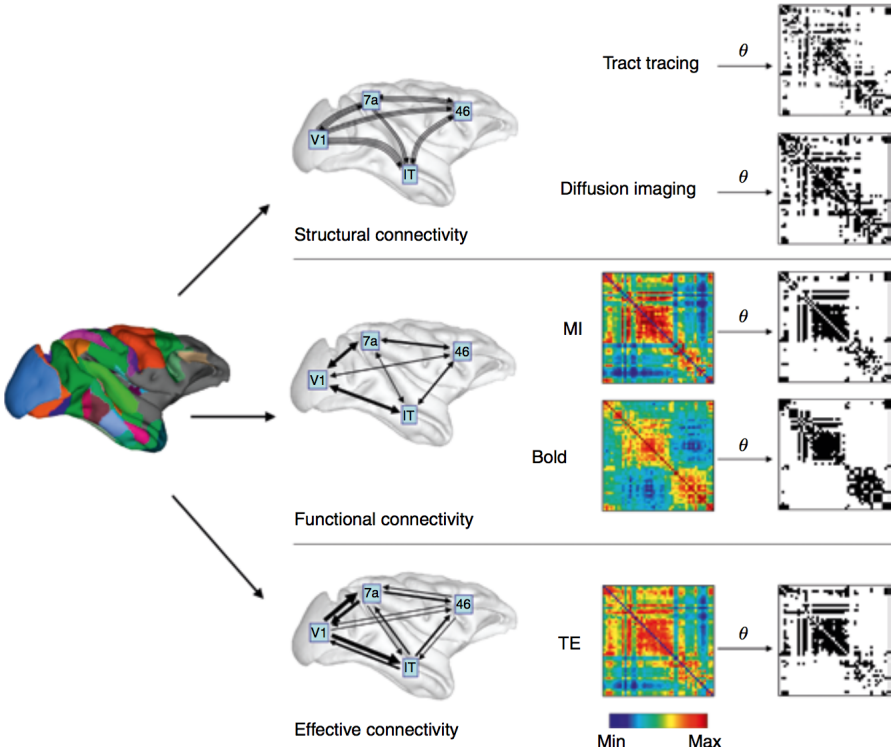

Figure 1.1: *Structural, functional, and effective brain connectivity. The image on the left displays a rendering of the parcelated macaque cortical surface, the middle column of plots shows schematic diagrams of structural connectivity (white matter pathways structurally linking brain regions), functional connectivity (statistical relations among brain regions), and effective connectivity (directed influences between brain regions). Plots on the right show weighted (in colour) and thresholded binary (black/white) matrices of structural, functional, and effective connectivity patterns*[1].

Structural connectivity refers to the plan of physical anatomical white matter connections linking different brain regions. White matter pathways and, their microstructural properties, can be quantified with magnetic resonance imaging (MRI), by using so-called diffusion weighted imaging (DWI) sequences. DWI datasets are analysed with diffusion tensor imaging (DTI), and

allow the characterization of the so-called structural connectome, integrated by nodes (specific brain regions acting as hubs) and links (white matter connections). DTI methods are insensitive to the directionality and do not inform in any way or manner about the level of functionality subtended by hard-wired anatomical projections. Therefore, they do not allow the extraction or inference of any meaningful functional information, neither do they uncover the features of the information flow and coding patterns running across them.

Functional connectivity refers to the statistical dependencies between neural activities in different brain regions regardless of their anatomical connectivity patterns. It can be characterized from either spontaneous and/or during task-driven brain activity. It is typically measured with functional magnetic resonance imaging (fMRI), a technique that considers the dynamics of increases and decreases in blood oxygen level-dependent (BOLD) signals from vessels supplying blood essentially to brain gray matter areas. These methods allow the characterization of different types of functional extended brain systems (such as, for example, the Default Mode Network and its different subsets) based on the mutual correlation of activity across different brain regions. A limitation of fMRI neuroimaging approaches, however, is the low temporal resolution at which we can measure these activations (in the order of 1 to several seconds), which is far slower than the time-scale at which a majority of neural mechanisms tend to occur (in the order of milliseconds).

Importantly, functional networks of interactions maintain a tight relationship with structural connectivity patterns, i.e., the structural connectome predicts the functional connectome. However, such relationship is not always straightforward. Indeed, functional interactions between two brain regions are not always subtended by direct structural white matter pathways linking those regions, but associated to indirect multi-synaptic long-range projections between the two sites.

Functional connectivity maps provide a set of 'mere' statistical relationships between activity patterns subtended by different brain regions, which are not necessarily causal. Indeed, a question that cannot be addressed with these procedures is to what extent the activity of two brain regions is crucial for information to flow into a network, other than being merely related statistically? What is the causal meaning of the statistical relationship? This question brings us to the concept of *effective connectivity*, which refers to the influence that neural systems hosted in a given brain region exerts over a second one, either at microscopic (synaptic activity) or macroscopic (regional excitability or activity levels of cortical/subcortical sites) levels. Therefore, the concept of effective connectivity provides information on directionality. This critical measure allows, for example, to show that the effect that a brain area "A" exerts over another brain area "B" might not be necessarily the same that area "B" exerts onto area "A". In a strict physical sense, causality relies on the identification of a cause and an effect, or, in other words, an event that originates (cause) a given response or a given consequence (effect) in general in a dose dependent (direct or inverse linear or non-linear) manner.

In a deterministic sense, the concept of causality can be either conceived in terms of temporal precedence and/or of physical influence. The *temporal precedence*-based definition of causality between two regions establishes that the activation of one of these regions must be preceded by the activation of another region. Nonetheless a more reliable manner to explore causality with regards to the influence of a brain region into another cerebral site consists on perturbing the activity pattern of a given site and observe whether such intervention influences the activity of a second site with whom we suspect subtends a causal interaction. The fundamental difference between these two definitions characterizes the different approaches employed to analyse causality. The temporal definition is the basis for the so-called Granger causality (see further explanations in the methods section of this dissertation). In contrast, the *physical definition* stated above is related to the notions of intervention and control[5], in which this work has been inspired.

1.2 EEG as a measure of connectivity

Functional and effective connectivity have been mainly studied using neuroimaging methods based on MRI recordings, as stated before. Despite being characterized as provided with an outstanding spatial resolution (in the order of several mm depending on voxel size and the influence of MRI field strength), the temporal resolution of the MRI BOLD signal, which mimics the activity of the different brain areas, is too slow (few seconds, depending on brain area and the tasks performed) to reflect the real dynamics associated with neuronal activation and signalling mechanisms, operating at the millisecond level.

A method that can overcome this limitation is electroencephalography (EEG). Using this technique, it is possible to record the electrical activity emerging from synchronous activations of neuronal population. There are different approaches to record EEG activity from the brain. The most common consists in recording EEG activity from the scalp (scalp EEG). This technique is performed through an electrode cap placed on the subject's head surface. It is a quite standardized and mainstream method in experimental and clinical applications. Nonetheless, the quality of the signal is limited given its sensitivity to be contaminated by non-biological electrical activity present in the environment, and to field distortion in sources of biological activity generated by layers of non-cerebral tissues (such as arachnoid mater, dura matter, skull bone and other subcutaneous layers, as well as the cerebrospinal fluid). placed between the signal source and the scalp EEG electrode[6].

During the last decade, additional technological approaches have been developed to overcome these limitations and record more spatially accurate patterns of brain activity. One of these methods is subdural electrocorticography (ECoG), a technique that involves the placement through a rather large craniotomy of two-dimensional grids of electrodes, which lay like a blanket, in direct in contact with the pial surface of specific cortical regions[7]. To note that, in humans, this technique, due to a high risk of infections, only allows recording either during neurosurgical operations, or for very brief periods of time before having to be extracted.

Another method is stereoelectroencephalography (sEEG) or intracranial EEG (iEEG), which consists on the placement of multi-contact electrode leads penetrating the brain[8]. Intracranial EEG enables the recording of local field potentials (LFP), i.e. compound potential product of the temporal and spatial summation of action potentials from clusters of neurons located in the vicinity of the contact. This approach is often used as a pre-surgical removal intervention in medication-resistant epilepsy patients, and allows for longer monitoring periods (1-2 weeks) than ECoG.

Independently of the specific method used to record EEG activity, measuring electrical activity in the brain allows to explore the underlying frequencies of brain oscillations present within the recorded signal. Local or widespread events of tonic or sustained oscillatory activity and synchrony, operating at specific frequency bands and cerebral sites have been found to encode for different cognitive processes such as attention, motor planning and memory, among others.

1.3 Entrainment of Brain Oscillations

A detailed and accurate comprehension of oscillatory phenomena is paramount for the fundamental and the clinical neurosciences. This is because neural oscillations and phase and/or frequency specific synchronization of cerebral sites within a network, can encode specific cognitive processes and behaviours, and be modulated through neural oscillatory entrainment, a procedure that consists in the progressive synchronization in time of an oscillation to an external source of energy such as electrical or magnetic stimulation[9]. Entrainment generated by a single stimulation source may operate locally, although entrained activity might also travel

throughout extended networks and hence modulate brain connectivity across large networks. In a scientifically or medically relevant diagnostic/therapeutic domains, these procedures could be used to impact coding mechanisms tied to normal/abnormal cognitive operations in which the targeted systems are involved and drive behavioural improvements For this reason, the development of non-invasive brain stimulation strategies (either focally via Transcranial Magnetic Stimulation, TMS; or widespread with Transcranial Alternating Current Stimulation, tACS) and their abilities to modulate patterns of local and inter-regional brain rhythmic activity by oscillatory entrainment, keeps spurring major attention and holds the promise to contribute to cognitive rehabilitation[10, 11] of functions such as perception, memory and attention, To better assess their impact, non-invasive stimulation techniques are generally combined with scalp EEG. Via the spread of entrainment across different nodes and brain regions, the network propagation of EEG signals, induced at a known frequency, have shown a potential to contribute to a causal exploration of connectivity via synchronization across different brain regions, a notion that lies at the core of the master project we conducted.

However, as indicated above, the use of non-invasive stimulation and recording methods, relies in uncertain measures, as their impact and mechanism of action and the anatomical sources remain unclear or difficult to predict. These limitations cast doubt upon the ability of rhythmic electrically/magnetic patterns to generate currents able to entrain frequency-specific oscillatory patterns on circumscribed cortical regions that can influence cognitive or behavioural activities.

Some of the limitations on studying the mechanisms underlying oscillatory entrainment are overcome in the current study by analysing data obtained with invasive stimulation methods known as Electrical Brain Stimulation (EBS) techniques. Deep Brain Stimulation (DBS), in which electrical pulses are delivered, via a neurostimulator implanted in the patients' brain, on highly circumscribed brain regions, and is used therapeutically in neurological and psychiatric disorders, such as Parkinson, severe depression, obsessive compulsive syndrome and epilepsy[12]. Although highly invasive, in contrast to TMS and tACS, DBS is a very focal stimulation technique, which can target directly a specific neural region or circuit, and modulate neurological or psychiatric symptoms in a way that is scalable, while the whole procedure is reversible by simply removing any implanted hardware.

In this context, a clinical approach and settings that could indirectly facilitate a more precise exploration of neural entrainment in awake humans through electrical brain stimulation, is the one provided by pre-surgical mapping of medication-resistant implanted human epilepsy patients (see Figure 1.2)[13, 14]. These clinical populations have their brain activity monitored to localize their epileptogenic foci (i.e., brain regions triggering epileptic seizures) to be eventually removed surgically thereafter. This is carried out through the implantation of arrays of intracerebral electrodes, improving through the use of causal or perturbation-based approaches, the localization of the seizing brain sources, hence helping to identify and limit the area considered for ulterior surgical removal, as to limit the potential cognitive collateral damage derived from such intervention. Interestingly, the multi-electrode arrays used for recordings can also be employed in clinically controlled settings to deliver highly focal patterns of direct electrical stimulation delivered at specific frequencies and intensities[8, 15]. Intracranial stimulation is performed systematically by pairs of contacts within each multielectrode, aiming to induce electrophysiological (iEEG based) generally subclinical seizures under controlled clinical conditions. By using this approach, clinicians are not exclusively forced to rely only on the onset of occasional spontaneous ictal events during localization of the epileptic region, but rather identify directly sensitive seizing sources by challenging them directly through electrical pulses. Each implanted region is causally surveyed to infer its ability to induce seizures. Combined with anatomical characterization of electrode location, such enhanced causal mapping approaches have the ability to contribute significantly to a more accurate identification of local epileptogenic activity evoked

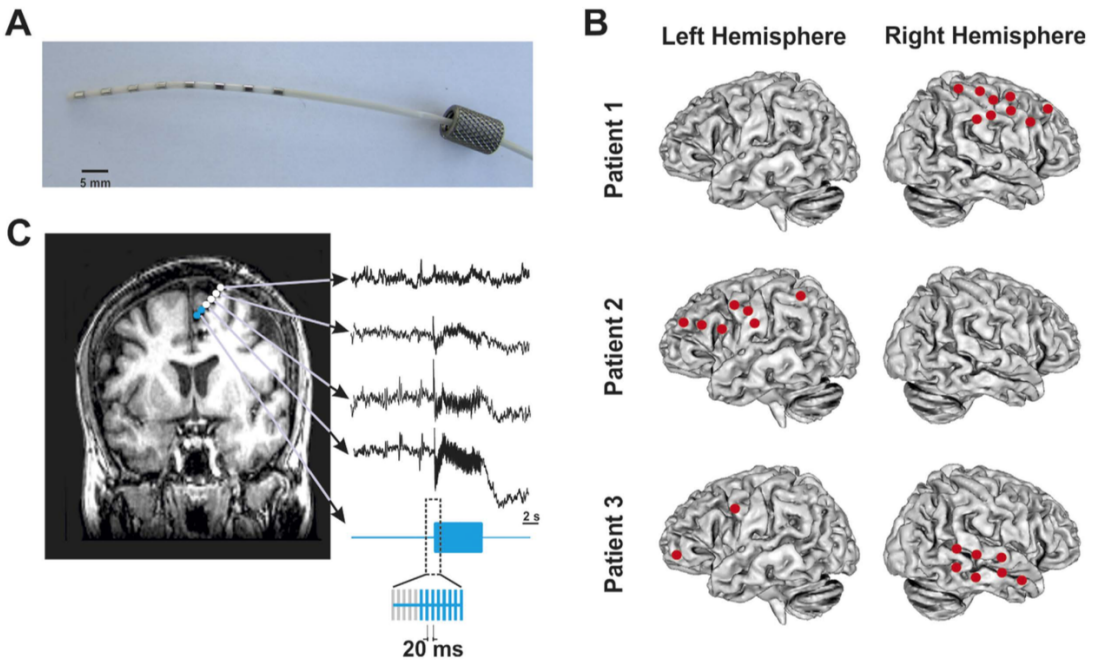

Figure 1.2: *Example of multielectrode implantations and intracranial stimulation procedures. (A) Image of an 8-contact intracranial multielectrode employed for stimulation and iEEG recordings. (B) Diagram of the implantation sites showing the location of every individual multielectrode in the brain of three single patients. (C) Detailed caption of a single multielectrode implanted in the frontal lobe of one of these patients, displayed on a T1 MRI scan (coronal view) recorded following implantation. Blue dots represent pairs of electrode contacts delivering 5 seconds long 50 Hz electrical bursts (blue iEEG trace). White dots signal the location of remaining contacts within the same electrode, recording brain iEEG activity concurrently with electrical stimulation patterns[2].*

and their sensitivity to synchronous frequency specific patterns.

Moreover, the short-lasting (5 to 10 seconds max at 1 Hz or 50 Hz) electrical stimulation bursts applied to local neural assemblies, which are routinely used to survey epileptic and non-epileptic regions, have the ability to entrain physiological oscillatory activity in a frequency which is dictated by the rhythm of the stimulation source[2]. Collaterally, this evidence supports the use of rhythmic stimulation in elucidating the causal contributions of synchrony to specific aspects of human cognition, and additionally to further develop the therapeutic manipulation of dysfunctional rhythmic activity subtending the symptoms associated with neuropsychiatric conditions.

Studies using isolated single pulse stimulation[16] or pulses extracted from intracranial low frequency patterns (1 Hz) have been also used to perturb networks. However, in absence of faster oscillation patterns driven by such electrical stimulation, data acquired with these procedures and the recording of cortico-cortical or cortico-subcortical evoked potentials (which can prove helpful to identify natural frequencies featured by specific brain locations, to probe direct connectivity or to estimate pathway distances between brain sites) does not grant the possibility to compile functional connectivity maps involved in the generation of frequency specific synchrony, deemed essential for information flow, information coding, and processing.

1.4 Research Questions

The general goal of this project is to develop, in a selected cohort of implanted patients, a method and procedure to causally characterize patterns of functional connectivity between brain regions

at resting-state or in response to frequency specific gamma stimulation. Such procedure will allow us in a near future, by adding similar datasets, to compile an accurate causal connectome of human brain under stimulation conditions as compared to resting-state. We will address this issue by assessing how frequency-tuned electrical currents delivered intracranially, in awake epileptic patients, induce enhancements of inter-regional synchrony within specific brain regions. The main question we are trying to decipher is whether, or not, these patterns hold any meaning when compared to functional connectivity patterns established under resting-state and to what extent functional connectivity synchronized causally at 50 Hz can be predicted by resting state connectivity. The knowledge that this project will generate might not improve intracranial brain stimulation procedures per se, but it will be instrumental to further understand and expand the use of oscillatory entrainment by means of invasive and non-invasive brain stimulation techniques.

Chapter 2

Materials and Methods

2.1 Patients

In this study, we performed our analyses on iEEG datasets obtained during individual sessions of direct intracranial stimulation delivered to medication-resistant patients (n=18) admitted to the Epilepsy Unit at the Pitié-Salpêtrière Hospital in Paris (France). Recordings were performed in the context of clinically guided causal mapping sessions aiming to localize and characterize epileptic foci prior to their neurosurgical ablation[13, 14]. Our patient cohort (10 female and 8 male, mean age 24.2 ± 4.3, range 18-29 years old) were implanted in different brain regions with intracranial depth electrodes (see Table 1-annex- for full details and demographic information). Implantation sites were exclusively planned and selected by epileptologists based on clinical criteria, not related with the final aims of the analyses performed for this dissertation and without any input from scientists.

Patients provided informed consent to any intracranial intervention, iEEG recordings and ulterior data analyses. All activities included in this project were performed under agreement from the INSERM, which sponsored the study and further approval by an independent ethical committee (CPPRB, Comité Consultatif de Protection des Personnes participant à une Recherche Biomédicale) Île-de-France I (reference number C11-16, 5-04). The Declaration of Helsinki and French and EU's regulations were respected at all times.

2.2 Multielectrode implantations for intracranial stimulation and iEEG recordings

For the above mentioned clinically guided causal mapping sessions, intracerebral multi-electrodes provided with 6 to 10 contacts (Adtech, Racione, Wisconsin, USA) were implanted and used concurrently either for stimulation or iEEG recordings (as shown in figure 1.2 included in the previous chapter). Contacts hosted by the same multielectrode were 2-3 mm long, 1 mm diameter length and spaced 5 mm apart from each other. Multielectrode implantation was guided with a Leksell stereotactic frame (Elekta, Stochkholm, Sweden). Isovoxel high resolution T1 MRI sequences (3T, General electric, Fairfield, Connecticut), performed prior to any intervention, served to plan the procedure, whereas a second T1 MRI and most importantly, a CT scan, carried out following the implantation procedure, was used to verify the site of each multi-electrode contact on each patient's brain and identify their MNI/Talairach standardized coordinates in normalized brain space.

2.3 iEEG recordings and datasets structure and configuration

During intracranial stimulation sessions, patients were fully awake and laid comfortably in a semi flexed position on a bed placed in a well-lighted room. Immediately prior, during and immediately following each stimulation trial, or during resting state iEEG recordings, patients were asked to remain relaxed and keep their gaze on a fixation cross, located in a screen placed in front of them. Two different iEEG datasets were considered for this study. The session started

by recording resting-state iEEG data simultaneously from all multielectrode contacts during three minutes (180 seconds).

After a short rest, the session involving recordings of iEEG activity, coupled to intracranial stimulation, started. Electrical stimulation was delivered in bursts of electrical pulses through a programmable clinical Micromed stimulator. The standardized clinical stimulation protocol consisted of electrical bursts made of 250 biphasic squared pulses (1 ms pulse width). Each pulse was delivered every 20 ms (i.e., at a 50 Hz frequency), giving rise to 5 seconds' length bursts. Electrical bursts were applied systematically through all pairs of spatially adjacent contacts hosted by the same multielectrode, using increasing intensities, from 0.5 to 8.0 mA, and delivered from the deepest to the most superficial contacts, or eventually vice-versa, upon decision of the epileptologist in charge of the mapping session. Continuous iEEG recording during the delivery of the electric bursts allowed the study of iEEG responses to electrical stimulation. These responses were recorded from multielectrode contacts not directly employed to deliver the stimulation, belonging to the same multielectrode, and by the contacts in the remaining multielectrodes of the implantation scheme. The neurologist in charge of the mapping session selected, on a case-by-case basis, which contact and which intensities were to be employed according to both the electrically evoked iEEG patterns and eventually the clinical responses reported by the patient. Inter-burst intervals were not strictly controlled in duration during the session, but were always kept longer than 45 seconds to avoid carry-over or build up excitability effects with the accrual of serially delivered electrical bursts[15].

The stimulation burst delivered during the above-described clinically-guided mapping sessions on epileptic patients were tuned to 50 Hz, which happens to be the frequency of the line-noise. 50 Hz stimulation was chosen as, according to empirical clinical observations, it is considered the frequency which is most likely to induce excitatory responses followed by a self-sustained after-discharge, when a seizure-sensitive area is hit by electrical stimulation[17], hence being the optimal stimulation frequency to maximize the chance of causally identifying epileptogenic sites and, at the same time, using the fewest electrical bursts, hence minimizing tissue damage by heat dissipation, and keeping evaluation sessions reasonably short.

Both intracranial iEEG datasets (from now on, RS-iEEG for resting state data, and Stim-iEEG for intracranial stimulation data) were recorded using the same 16 bits Micromed Amplifier system (Micromed, Mogliano Veneto, Italy). Sampling rate was set to 1024 Hz and the signal was band-pass filtered during the acquisition at 0.15-350 Hz. An external electrode located on the scalp FCz position (10/20 EEG system), was used as a recording reference.

2.4 Stimulation iEEG dataset pre-processing

Prior to the automated pre-processing of the iEEG data, recorded signals from each multielectrode contact were visually inspected to determine whether recordings had been successfully acquired. Contacts whose delivered signals were either contaminated with noise or unlikely related to any biological source were taken off from the analyses for both RS-iEEG and Stim-iEEG datasets. Excluded signals accounted for 4.8 % of the total number of recordings considered in the study. A pre-processing custom-made script, based on in-house software and coded in Matlab (Mathworks, MA, USA) was developed. Pre-processing steps included procedures for electrical artefact removal, iEEG time series segmentation, the re-ferencing of iEEG signal and their differentiation on the basis of stimulation intensity.

2.4.1 Artifact Removal and Segmentation of iEEG Signals

For the Stim-iEEG dataset, every recorded iEEG stimulation signal contained a patterned artifact made of high-amplitude waveforms which lasted for 8 ms after each electrical pulse. This

artefact was removed by cutting off 8 ms epochs of iEEG signal following pulse onset, and by interpolating the missing signal using a weighted cubic spline method[18, 19].

For each stimulation trial, data were segmented in periods of 15 seconds (5 s prior and 10 s following the onset of the burst, including burst duration).

2.4.2 Referencing of iEEG Signals

The quality of the signal recorded from the reference electrode during iEEG recordings is paramount to avoid contamination that may negatively influence outcomes or alter analyses. Additionally, the close vicinity of the multielectrode contacts explains the similarity of recordings acquired via spatially adjacent contacts, hence likely exposed to the same source, and, therefore, running into the risk of overestimating connectivity values. In order to get rid of such undesired effects, a Laplacian method consisting in re-referencing the signal recorded by each contact to the signal from neighbouring multielectrode contacts with the calculation of the local field potential (second spatial derivative[20]) was applied to both iEEG datasets.

Since the multielectrodes' contacts are organized along serial strips, the number of neighbouring contacts were either 1 or 2, depending on the contact's position within each multielectrode. Contacts located in the superficial or towards the tip of the multielectrode were only adjacent to a single contact (in contrast to the remaining ones, which could all be paired to a second contact). In the latter case, the local field potential second spatial derivative was estimated using the following equation:

$$x_n(t) = x_n(t) - \frac{1}{2}(x_{n-1}(t) + x_{n+1}(t)) \tag{2.1}$$

with $x(t)$ being the time-series for contact n. For contacts adjacent to only one other contact, the applied procedure simply consisted in subtracting from its signal the signal of the adjacent contact.

The contacts used to deliver the electrical bursts were not considered for the n series (see equation2.1), as no signal could be recorded by such contacts during the stimulation. The same procedure was applied when the signal of an adjacent contact had to be removed from the analysis due to contamination.

2.4.3 Differentiation according to the intensity of electrical gamma stimulation

Since intracranial stimulation was applied at different intensities (ranging from 0.5 to 8 mA), potentially inducing different effects, iEEG data were clustered based on the stimulation intensity as those obtained under low intensity stimulation and those influenced by high intensity stimulation. The first dataset comprised all stimulations delivered at intensities equal or lower than 1.0 mA (56.29 % of the total stimulation time series) whereas the second dataset included iEEG from stimulation events delivered at intensities higher than 1.0 mA (43.71 % of the total time series). This approach to classify and analyse data addressed the fact that the use of high stimulation intensity at levels higher than 1.0 mA varied very unevenly across electrode contacts and participants. In other words, while low intensity stimulation was delivered through almost all pairs of multielectrode contacts, that was not the case for stimulation delivered at an intensity higher than 1.0 mA (which were only employed in the eventuality that the neurologist in charge of the on-going session deemed those clinically necessary). Hence, in order to avoid influence of high intensity stimulation iEEG recordings (that only existed in only certain regions), datasets were divided in these two groups, having low intensity iEEG stimulation the lowest common intensities, in order to diminish the variability of the dataset.

2.5 Resting state iEEG dataset pre-processing

We applied the same procedure for removal of contacts with signals either contaminated by noise or recording signal from non-biological sources, as described in the section 2.4. A pre-processing script written using in-house software and coded in Matlab (Mathworks, MA, USA), similar to the one used for the Stim-iEEG dataset (see section 2.4), was employed for data processing. Differently, however, since no stimulation was delivered during such resting state recordings, pre-processing steps included only procedures for epoching, segmenting and referencing the signal.

2.5.1 Epoching and segmentation of iEEG signals

The Resting-state iEEG dataset was individually segmented in 90 consecutive 2 seconds epochs, which were then averaged, thus obtaining a representative 2 seconds iEEG signal trace from each contact.

2.5.2 Referencing of iEEG signals

The same procedure reported for the Stim-iEEG dataset, based on the use of a Laplacian method, followed by the referencing of the signal (see section 2.4.2), was applied. Nonetheless, there was no need to consider stimulation contacts, as there were none that were affected by this case.

2.6 Anatomical co-localization of contacts

Contacts were grouped in discrete regions according to the Automated Anatomical Labeling (AAL) atlas[21], which is divided as shown in figure 2.1. The standardized MNI coordinates of each multielectrode contact were determined by normalizing each individual MRI volume into MNI space, whereas the AAL atlas region was used to identify in which anatomical parcelation (area, region or site) the contact was placed. In our cohort (across different patients, see Table 1, in Annex), multielectrode contacts were present in 62 of the 116 cerebral regions featured in the AAL atlas.

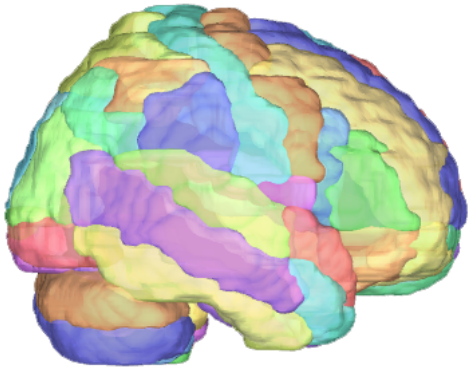

Figure 2.1: *Regions comprising the AAL Atlas*

Intracranial EEG signals recorded by contacts of the same patient which fell within the boundaries of the same AAL region were averaged across, yielding a single representative time series per region for each patient for each dataset (RS-iEEG and Stim-iEEG).

2.7 Mathematical methods for analysis

Different mathematical approaches, considering the properties of iEEG time series, are available to compute functional and effective brain connectivity maps[22–24], and allow the compilation of the so-called adjacency matrixes between region pairs. The iEEG analyses methods employed in this study can be divided in three groups: time-based methods, information-based methods and frequency-based methods.

2.7.1 Time-based

Time-based methods are based on measuring the similarity of two different time-series as a function of a parameter called 'time-lag'. Roughly speaking, they consist in comparing a given time series with the 'past' or the 'future' of a second time-series. Since iEEG time-series are non-linear, it is necessary to use specific analytic tools that fulfil and respect this condition. We used the nonlinear correlation coefficient, which is defined as the maximum of the following equation:

$$h^2_{xy}(\tau_{xy}) = \frac{\sum_{k=1}^{N} y(k+\tau_{xy})^2 - \sum_{k=1}^{N}(y(k+\tau_{xy}) - f(x(k)))^2}{\sum_{k=1}^{N} y(k+\tau_{xy})^2} \tag{2.2}$$

where f is a nonlinear fitting curve that approximates the statistical relationship between the signal x and y.

This measurement can be combined with the direction index[25], which is computed with the nonlinear correlation coefficients h^2_{xy} and h^2_{yx} and their time delays τ_{xy} and τ_{yx} (as follows):

$$D = \frac{1}{2}(sgn(\Delta h^2) + sgn(\Delta\tau)) \tag{2.3}$$

To measure similarities on RS-iEEG activity from different regions, h^2_{xy} was pair-wise measured by using equation 2.2, computed using x and y as signals from different regions. These measurements, computed for each patient, allowed us to establish weighted adjacency matrixes for each patient (see fig. 2.2a) modelling the patient-based connectivity between the implanted regions. In order to determine which of these connections were meaningful, we thresholded each adjacency matrices using a density threshold that filtered out the weakest links between regions. The threshold value was based on a recently validated criterion[26] that maximizes the ratio between the overall efficiency of a network and its wiring cost. This criterion establishes that the average node degree (the number of edges connected to a node) has to be approximately 3, which leads to a total number of edges, m, in the connectome, that scales as $m = (3/2) * n$, with n being the number of nodes. Following this relation, the weakest edges were filtered out, obtaining a binarized version of the adjacency matrix including only the significantly meaningful edges. Using equation 2.3, the directionality of the information was assessed.

Since one of the main aims of the study was to compile a functional connectivity atlas of the human brain on the basis of resting-state iEEG data from every AAL region present in at least a single patient, individual connectomes were integrated in a whole population adjacency matrix, representing connectivity between regions across every patient. To that end, every pair-wise weighted h^2_{xy} values (for each non-linear correlation coefficient between signals from region x and y), of datasets from AAL regions that were present at least twice in the same patient, were averaged across. Thus, an RS-iEEG adjacency matrix with a non-linear correlation coefficient for each pair-wise edge was obtained (see fig. 2.2b).

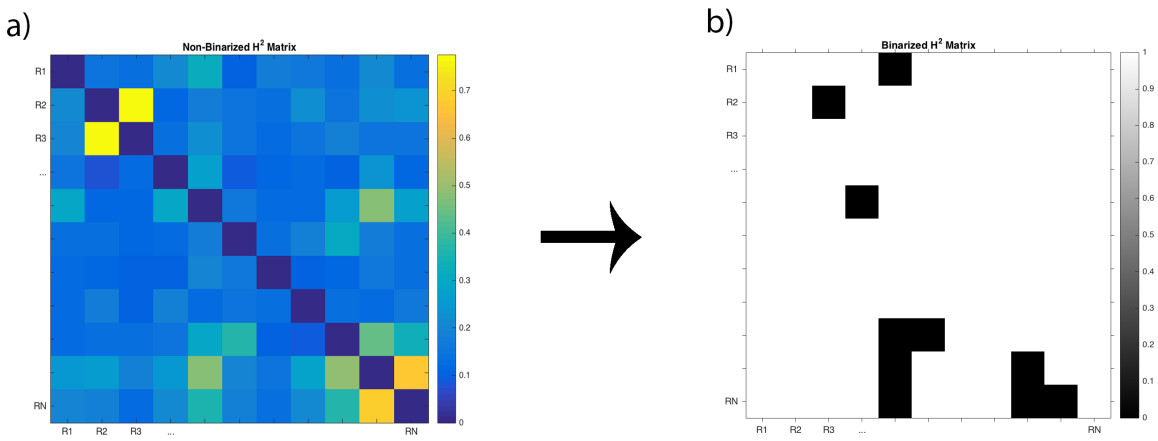

Figure 2.2: *(a) example of a weighted adjacency matrix for h2 values, in which every pair-wise edge has a value from 0 to 1. The diagonal of the matrix is set to 0, and represents the pair-wise edge between the pairs of the same region; (b) example of the adjacency matrix from the same dataset shown in (a) after thresholding and binarization, where the only values left are the ones that represent a meaningful connection (and are all set to 1) and every other value is 0.*

2.7.2 Information-based approaches: mutual information index

Another method to compare two iEEG signals consists in using information-based measures. These are based on the concept of Shannon entropy, which can be defined as the expected value of the information contained in each signal. We define Shannon entropy as:

$$I_X = \sum_x p_x(x) log \frac{1}{p_x(x)} \tag{2.4}$$

Wherep_x is the probability of character number x showing up in a stream of characters of the given "script". If we now consider two random variables X and Y, we can estimate their mutual dependence (mutual information), as the average amount of code necessary to encode the draws of a signal X using another signal Y, using the following equation:

$$MI_{XY} = \sum_{xy} p_{XY}(x,y) log \frac{p_{XY}(x,y)}{p_x(x)p_y(y)} \tag{2.5}$$

Although mutual information does not take into account potential asymmetries between pairs of iEEG time series, the analysis of resting-state data followed the same procedure reported for non-linear correlation coefficient, h^2_{xy}, reported in section 2.7.1. The same type of weighted adjacency matrixes was calculated, and the above-reported procedure to threshold them was employed (see fig. 2.2). Moreover, since mutual information indexes do not permit estimations of directionality, the sense of direction (which node was the driver and which one the follower) in which information flowed remained undetermined from these analyses.

2.7.3 Frequency-based Methods

In order to provide a causal or perturbation-based estimate of the functional strength linking the two brain regions, we also computed functional connectivity measures (and aimed to compile an atlas thereof) during episodic rhythmic entrainment with intracranial 50 Hz short electrical bursts (as compared to prior and following) between the region being stimulated and a second brain region (see our Stim-iEEG dataset). This type of functional signature was defined

in our Stim-iEEG dataset as the enhancement of frequency specific local oscillatory activity, phase-locked (i.e., synchronized in phase) to individual pulses integrating the source of rhythmic electrical stimulation[2, 10], during the 50 Hz burst delivery period. The enhancement of oscillatory activity was defined by (1) an increase of 50 Hz power during the stimulation period, and (2) enhanced and sustained phase-coupling between the induced rhythmic activity and the output of the stimulation[10, 27]. We extracted time-frequency maps by convoluting each reference-free iEEG signal with a complex Morlet wavelet[28, 29]:

$$W(t, f_0) = (2\pi\sigma_t^2)^{-\frac{1}{2}} e^{\frac{-t^2}{2\sigma_t^2}} e^{2i\pi f_0 t} \tag{2.6}$$

in which the relation $\frac{f_0}{\sigma_f}$ (where $\sigma_f = \frac{1}{2}\pi\sigma_t$ was set to 6.7[28]. These measures were computed on frequencies from 1 to 100 Hz, in 1 Hz steps. As we were interested in measuring increases of power and/or phase coupling, we calculated the percent change compared to baseline [-300 to -100 ms], prior to burst onset in the 45-55 Hz frequency band. However, these measures do not reflect the extent to which electrically induced gamma oscillations are time-locked to the electrical pulses delivered by the intracranial electrical stimulator. The temporal dynamics of the instantaneous phase, between the electrical output delivered by the two stimulation contacts on each electrical burst and the 50 Hz-component of each of the iEEG time series recorded within the stimulating multielectrode, were computed for each time series. Only contacts showing average power increases in the [45-55 Hz] band during the stimulation period 10 times higher than the pre-stimulation onset baseline were considered. A modelled signal emulating the 50 Hz pattern delivered by the electrical stimulator was generated using an in-house script in Matlab (Mathworks, MA, USA). Artificially generated signals had the same length and sampling rate (1024 Hz) as the original data, with the value "+1" (followed by a "-1" to account for its biphasic waveform) taken at the onset of the electrical stimulation, and repeated every 20 ms for the duration of the stimulation epoch, whereas a value of "0" was added everywhere else along the time series. We calculated the instantaneous phase difference by comparing the modelled quadratic waveform emulating the 50 Hz burst delivered by the electrical stimulator with the gamma [45-55 Hz] iEEG components (post-artifact removal) recorded by each multielectrode contacts of the implantation scheme[2]. We computed for each pair of the above-described time-series (using the Morlet wavelet coefficients of the modelled stimulator output signal and the iEEG recordings for each contact not involved in the stimulation) the phase difference, and estimated during 50 Hz stimulation the phase-synchrony, between these two signals. To that end, we applied the equation shown below:

$$e^{[i(\varphi_z(f,t)-\varphi_x(f,t))]} = \frac{W_x(f,t)W_x^*(f,t)}{|W_x(f,t)||W_z(f,t)|} \tag{2.7}$$

where W represents the Morlet coefficient for each frequency f and time t; x and z are each of the two signals (iEEG and the stimulator) and phi_x and phi_z their instantaneous phase[30].

To measure the consistency over time of the phase difference between these two signals, the single-trial phase-locking value (S-PLV)[31] described by the following equation, was calculated:

$$SPLV = |\frac{1}{\delta}\int_{t-\delta/2}^{t+\delta/2} e^{[i(\varphi_z(f,\tau)-\varphi_x(f,\tau))]} d\tau| \tag{2.8}$$

where *delta* represents a time period covering a specific number of cycles within the frequency of interest. Following recommendations[30, 32], it was used $delta = 200$ ms, which corresponded to 10 cycles of the 50 Hz frequency of interest, which is the one at which the bursts were delivered. The S-PLV informs on the stability of the phase difference during a single trial (i.e., considering it a single measurement) and its values ranged from 0 (random fluctuations

of phase-difference) to 1 (indicating the strongest phase-locking possible). To determine which S-PLV values would account for the two most relevant 5-second-long periods, i.e., baseline of 5 seconds prior to stimulation (pre-stimulation) and 5 seconds during stimulation (stimulation), each of these periods was divided into 5 x 1 second windows. The highest S-PLVs for each 1 second window were singled out and the 5 highest S-PLVs (one for each 1-second window of iEEG activity) were averaged across. The final average of such 5 highest mean S-PLV was taken as a representative estimate of the pre-stimulation and the stimulation 5 second periods. This approach, which is exemplified in fig. 2.3, was used to limit variability in the S-PLVs.

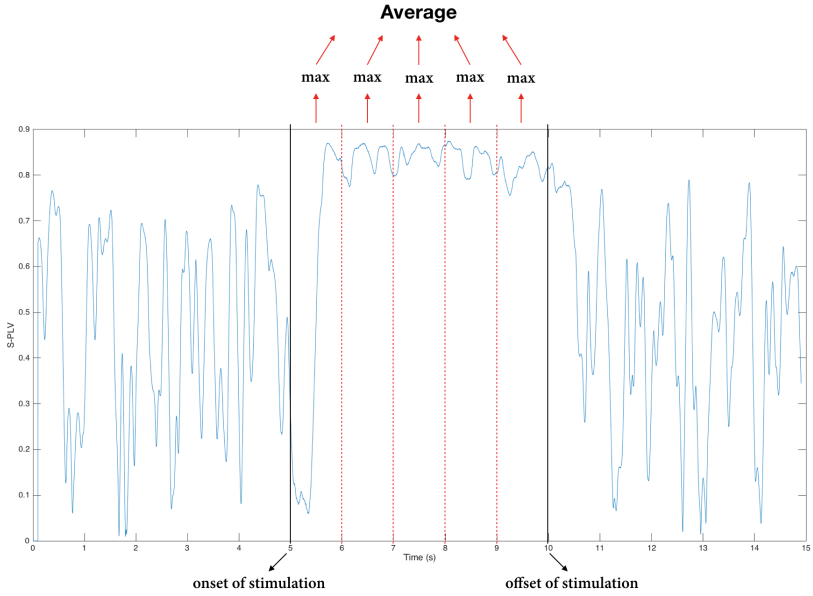

Figure 2.3: *Method applied to determine mean S-PLV representative for the pre-stimulation or stimulation periods for Stim-iEEG datasets. Each 5 seconds' long period (pre-stimulation and stimulation periods) were subdivided into 5 x 1 second periods in the highest S-PLV was singled out. The highest S-PLV value of each 1 second windows were averaged through, yielding a representative estimate for the whole 5 second period.*

Given our interest in measuring increases of S-PLV by comparing iEEG recordings obtained prior and during stimulation, pre-stimulation representative S-PLV estimates calculated as indicated above were used as baseline to normalize the representative S-PLVs for the stimulation period. Normalization was performed by subtracting the former from the latter (i.e., S-PLV during stimulation – S-PLV prior to stimulation)[33]

Similarly to what has been described in sections 2.7.1 and 2.7.2, we built an S-PLV connectivity matrix, which included data from every patient of our cohort, for both low and high intensity Stim-iEEG datasets. Considering data only from stimulation trials in which pairs of adjacent contacts delivering electrical current were both within the boundaries of the same AAL region (hence excluding time series in which this might not have been the case), the representative S-PLVs of different patients associated to pairs of time series stimulated on and recorded from the same AAL region were averaged through, in order to end up with a final single S-PLV value for each pair-wise edge probed with stimulation representing the cohort of studied patients. This procedure was conducted for every region in which stimulations bursts were delivered (n=42 stimulated/iEEG sampled regions). Since not every AAL region considered in the Stim-iEEG

dataset were stimulated, note that the number of regions of the stim-iEEG mapping was lower than those present in the RS-iEEG dataset (n=62 iEEG sampled regions).

Using the same thresholding approach and criteria mentioned previously (see sections 2.7.1 and 2.7.2) our weighted S-LPV matrix, of 43 regions, was binarized (1 vs. 0) via S-PLV values, by assigning a value of 1 only to the relevant connection edges and a value of 0 to the remaining ones that did not fulfil this condition. Directionality was assessed based on the assumption that information had to necessarily flow from the region where the electrical stimulation was delivered towards any remaining AAL brain region or regions hosting at least a multielectrode contact.

To compile the group RS-iEEG functional connectivity maps comparable (in spite of obvious differences in the number of nodes and edges and the use of stimulation only in the Stim-iEEG dataset) to those obtained during gamma electrical stimulation, S-PLV calculations were also conducted for the RS-iEEG dataset using the same main procedure described for Stim-iEEG maps in the preceding paragraphs. Instantaneous phase differences between the gamma [45-55 Hz] iEEG components at rest were computed. Nonetheless, since, RS-iEEG datasets were recorded at rest in absence of stimulation bursts, we were unable to use the exact same above-mentioned metrics (and in particular to compare functional interactions between the pulses delivered by the stimulation bursts and iEEG activity from AAL regions hosting at least a recording contact). Instead 2-second iEEG signals estimated for all pairs of AAL regions were compared across. As previously done for Stim-iEEG datasets, the consistency over time of the phase difference (S-PLV) between each pair of time-series was again computed using the above-mentioned equation 2.8. In contrast with the procedure applied to Stim-iEEG dataset (for which the average of the 5 highest S-PLV extracted from 5x 1-second windows was taken as the representative S-PLV measures for each 5-second pre- and stimulation periods), for RS-iEEG data we estimated the representative S-PLV as the arithmetic mean of instantaneous SPLV across each complete 2-second-long RS-iEEG signals.

2.8 Brain Map construction

Individual and group functional connectivity maps (functional connectomes), for both resting-state (RS-iEEG) and stimulation – high and low – (STIM-iEEG) datasets, were constructed using NeuroMArVl (Monash University, Melbourne, Australia). This is a browser-based software to produce graphic renderings of brain connectomes. For such representations, the MNI coordinates attributed to each AAL regions from which data were included in the connectome (hence being a node of the graph) were estimated as the mean between the MNI x, y and z coordinates of the contacts whose iEEG or stimulation modelled signals had been averaged as representative for that region. Benefitting from its ability to provide directionality information (i.e., which node of given interaction is likely to drive/or lead and which one follows), the binary matrices employed to represent functional connectivity maps for RS-iEEG dataset were based on the non-linear correlation coefficient (h^2_{xy}). Additionally, however, S-PLV based RS-iEEG connectivity maps were also computed to facilitate (in spite of the many differences between the two) a qualitative/quantitative comparison between connectomes compiled on the basis of the RS-iEEG and Stim-iEEG datasets. The functional connectomes based on Stim-iEEG dataset were only constructed using S-PLV datasets.

2.9 Topological properties of the networks

To provide a more quantitative comparison between the different resting state and stimulation connectomes, we opted for calculating the node degree. This topological outcome descriptive

measure estimates the number of edges connected to a single node within a connectome. For an adjacency matrix A, the degree for a node indexed by I in an undirected network is defined as:

$$k_i = \sum_j a_{ij} \tag{2.9}$$

where the sum is calculated across each node within a given connectome.

In the case of a directed network, each node has two degrees, an out-degree and an in-degree. The first is the number of outgoing edges emerging from a given node defined as follows:

$$k_i^{out} = \sum_j a_{ji} \tag{2.10}$$

and the second is the number of incoming edges onto a node calculated by using the formula below:

$$k_i^{in} = \sum_j a_{ij} \tag{2.11}$$

The total degree of a node in a directed network is, then, the sum of its in-degree and out-degree:

$$k_i^{tot} = k_i^{in} + k_i^{out} \tag{2.12}$$

2.10 Statistical Analyses

Non-parametric Spearman rank tests were used to estimate the statistical significance of the correlations between h_{xy}^2 and S-PLV in resting-state data (i); h_{xy}^2 and S-PLV for both low and high intensity stimulations (ii); h_{xy}^2 and 50 Hz pre vs. during stimulation power increases for both low and high intensity electrical gamma (50 Hz) stimulation (iii); S-PLV in resting-state data and S-PLV for both low and high intensity electrical gamma stimulation (iv); S-PLV in resting-state data and Power for both low and high intensity electrical stimulation (v); S-PLV for both low and high intensity stimulation and 50 Hz power pre vs. during stimulation increases for both low and high intensity electrical gamma bursts (vi), S-PLV for low intensity electrical stimulation and SPLV difference for high intensity electrical stimulations (vii), and pre vs. during stimulation power increases for low intensity and also for high intensity electrical gamma bursts (viii). For all tests, significance level was set at $p < 0.05$.

Chapter 3

Results

3.1 Stimulation iEEG-based connectome

To facilitate a better understanding of the complex and long series of analysis we performed, our results will first be presented on a dataset of a representative patient (n=1, patient reference no. 1998), followed by the results for the whole population of epileptic patients (n=18) analysed for this dissertation.

3.1.1 Example of a single patient connectome

Patient reference number 1998 had multielectrode contacts implanted in the following 11 AAL regions of the right hemisphere and the cerebellum: Supramarginal Gyrus, Angular Gyrus, Inferior Parietal Lobule, Middle Occipital Gyrus, Superior Temporal Gyrus, Fusiform Gyrus, Inferior Temporal Gyrus, Middle Temporal Gyrus, Lobule III of Cerebellar Hemisphere, Crus I of Cerebellar Hemisphere and Inferior Occipital Cortex (number of contacts on each region and additional information are presented at the table annexed). Connections between regions were established pair-wise on the basis of our established criteria for enhanced neural entrainment. We considered regions that showed both increase of S-PLV and 50 Hz power at least 10 times higher than base-line pre-stimulation values (see methods section for details). As we divided electrical stimulation in two different groups based on the intensity, two different connectivity maps, one for high and one for low stimulation intensity, will be presented.

The *High Intensity Stim-iEEG connectome* of patient reference 1998 is represented in the figure 3.1. In this S-PLV based connectome, we observe the nodes and edges that are based on the criteria described in the section 2.7. The Right Inferior Occipital Cortex is a node that shows oscillatory entrainment when the stimulation is delivered to any other implanted region (hence a 'receiver' region). Therefore, directed connections from other regions of the network to this region can be observed. In this context, information is considered to flow inwards into the node. When the opposite happens (i.e., when the stimulation is delivered to this region and other regions show oscillatory entrainment), the region is considered to send information outwards, thus being a 'sender'. Links in this category are considered to flow outwards of the node. Regions, such as Right Middle Occipital Gyrus, Right Lobule III of Cerebellar Hemisphere, Right Crus I of Cerebellar Hemisphere, Right Inferior Parietal Lobule and Right Superior Temporal Gyrus, only have outward links, sending information (hence in this case of stim iEEG dataset, entraining gamma oscillations) onto other regions and not receiving any information.

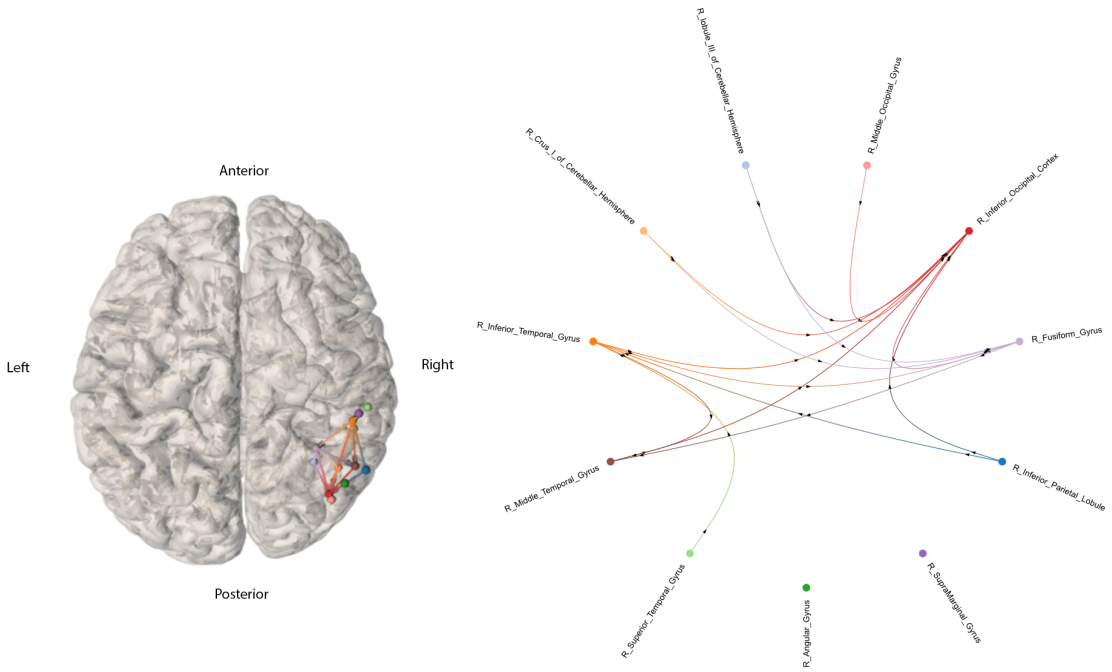

Figure 3.1: *High Intensity Stimulation iEEG-based connectome, from patient reference 1998 (n=1) displayed on a normalized brain volume or as a graph, estimated with S-PLVs. (Left panel) 3D connectome is represented in a normalized brain template, with each node corresponding to an implanted AAL region. The geometrical location of each node is placed on the average MNI location of the contacts that were localized as located in the same AAL region. (Right panel) Connectome represented as a circular graph with all nodes located equidistantly (importantly, neither node location or edge length inform about the distance between two nodes). Nodes correspond to each implanted AAL region. In both graphs, arrows added to each edge represent the estimated direction of the signal spread from the electrically stimulated region to a second one.*

Two different regions, the Right Angular Gyrus and Right Supramarginal Gyrus do not exhibit signs to subtend functional connectivity with any region of the connectome. This suggests that, at least for the regions sampled and considering our astringent criteria for entrainment, when stimulation is delivered onto these regions, such patterns are not conveyed to other parts of the connectome (hence remaining regions that show no signs of oscillatory entrainment), and moreover, that when other regions are stimulated, these two cerebral cites remain uninfluenced (hence no oscillatory entrainment is imposed on them at the gamma frequency).

As for the *Low Intensity Stim-iEEG connectome* (figure 3.2), from the same patient, differences such as the absence of some links (edges) present in the high intensity stimulation connectome can be observed. The most relevant is the absence of any link, either outwards or inwards, for the Right Fusiform Gyrus to any of the sampled regions hosting multielectrode contacts. Some other connections present in the High Intensity Stim-iEEG Connectome are absent in this low intensity one, but regions, such as the Right Inferior Occipital Cortex, display a similar status to that shown when stimulated with high intensity currents. Four different regions exhibit no signs of connectivity (no connections between these regions from and to the rest of implanted regions).

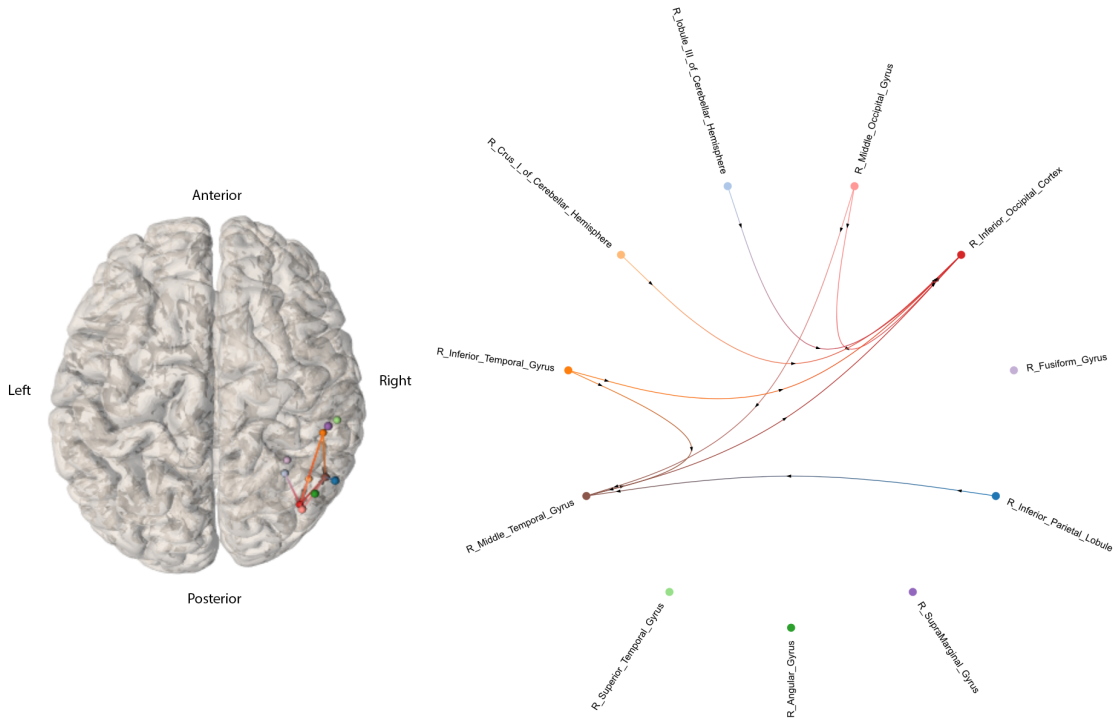

Figure 3.2: *Low Intensity Stimulation iEEG-based connectome, from patient reference 1998 (n=1) based on S-PLVs. On the left side, a 3D connectome is represented in a default intact brain template in normalized space, with each node corresponding to an implanted AAL regions. The geometrical MNI node location represents the average x, y and z coordinates of the contacts hosted on the same AAL region. On the right side, the connectome is represented via a circular graph. Nodes correspond to each implanted AAL region. On both graphs, arrows in the edges represent the estimated direction of the signal spread (see caption from prior figure for further explanations or details)*

When the adjacency matrixes from both the *High Intensity Stim-iEEG connectome* and the *Low Intensity Stim-iEEG connectome* are subtracted one from the other, it is possible to determine which edges are specific from each connectome. As observed in figures 3.3 and 3.4, only 3 edges present in the Low Intensity Stim-iEEG Connectome are specific to this connectome, hence not present in the high intensity one. These three edges have the Right Middle Temporal Gyrus operating as 'receiver', with the Right Middle Occipital Cortex, the Right Inferior Occipital Cortex and the Right Inferior Parietal Lobule, as 'senders'.

When considering the opposite, i.e., links proven to be specific for the High intensity Stim-iEEG connectome, hence not present in the low intensity Stim-EEG connectome, 8 additional edges showing different nodes and different directions, appeared and were added to the network of this patient at higher intensity levels.

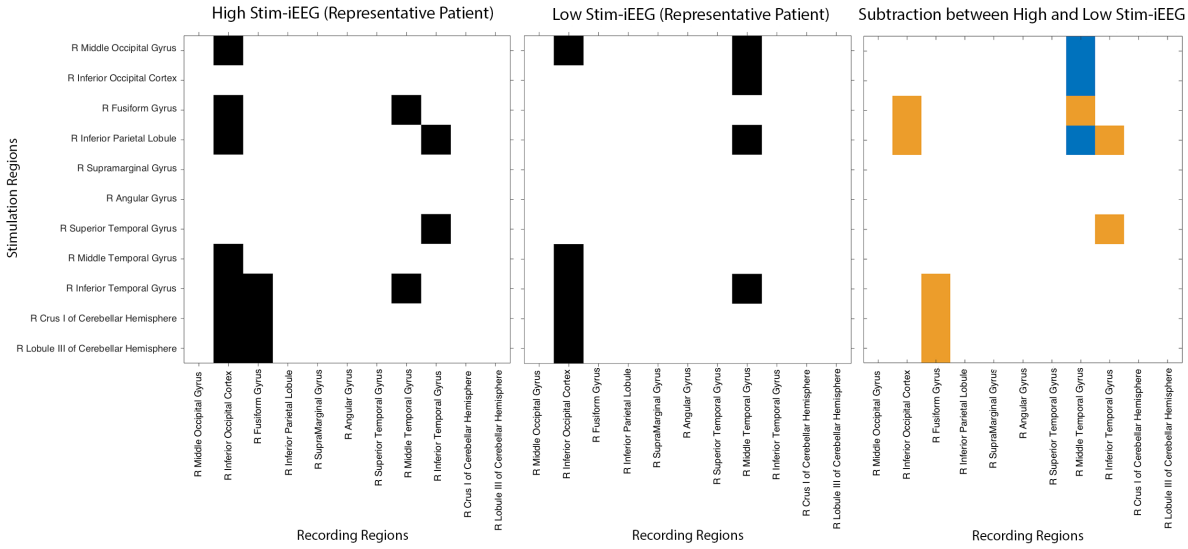

Figure 3.3: *Comparison of adjacency matrices for patient ref. 1998 (n=1) based on S-PLVs. In (a, left, in black) and (b, center, in black), edges are represented in black, whereas matrix (c, right) displays the edges present either only during high intensity stim-iEEG (orange cells) or exclusively during low intensity stim-iEEG (blue cells).*

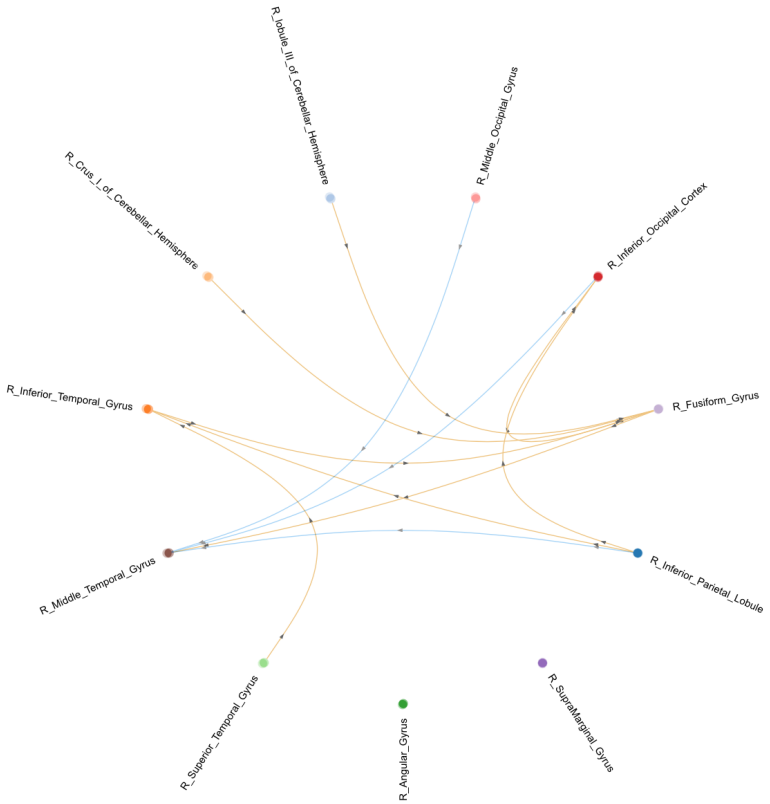

Figure 3.4: *Circular connectome with equidistally represented nodes, associated to prior adjacency matrices based on S-PLVs for patient ref. 1998 (n=1), showing the edges present either only during high intensity stimulation iEEG datasets (in orange) or only during low intensity stimulation (in blue).*

3.1.2 Whole population connectivity atlas or connectome

By merging, in a common normalized MRI space, iEEG functional connectivity data from every individual S-PLV based single patient connectome, we build a connectomic model for the entire population of n=18 implanted patients included in our cohort. For the complete dataset, the total number of stimulations (hence iEEG time-series) was 2360. These were delivered through a total of 389 contact multielectrode pairs (mean of 21.68.48 per patient, range between 6 and 40), and recorded from 928 total contacts, ruling out contacts present in non-encephalic regions not represented in the AAL atlas parcellation. A total of 360992 iEEG time-series were considered in our analyses.

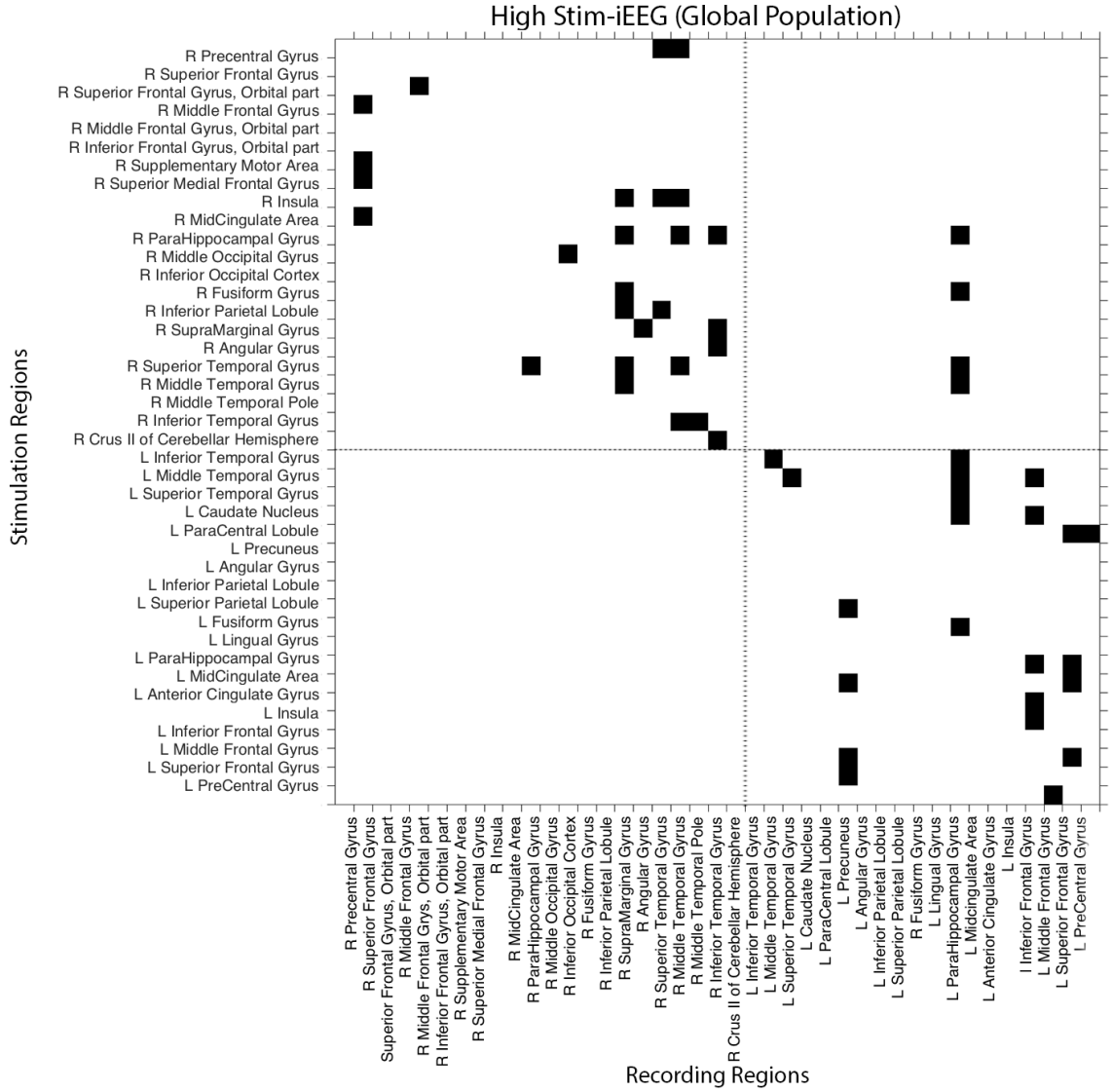

Figure 3.5: *High Intensity Stimulation-iEEG Connectome Adjacency Matrix for the complete population of patients (n=18) based on S-PLVs. The horizontal and vertical dotted lines divide the brain regions belonging to the left or the right hemisphere. Black cells represent a pair-wise connection that fulfilled criterion for gamma (50 Hz) S-PLV increases during stimulation.*

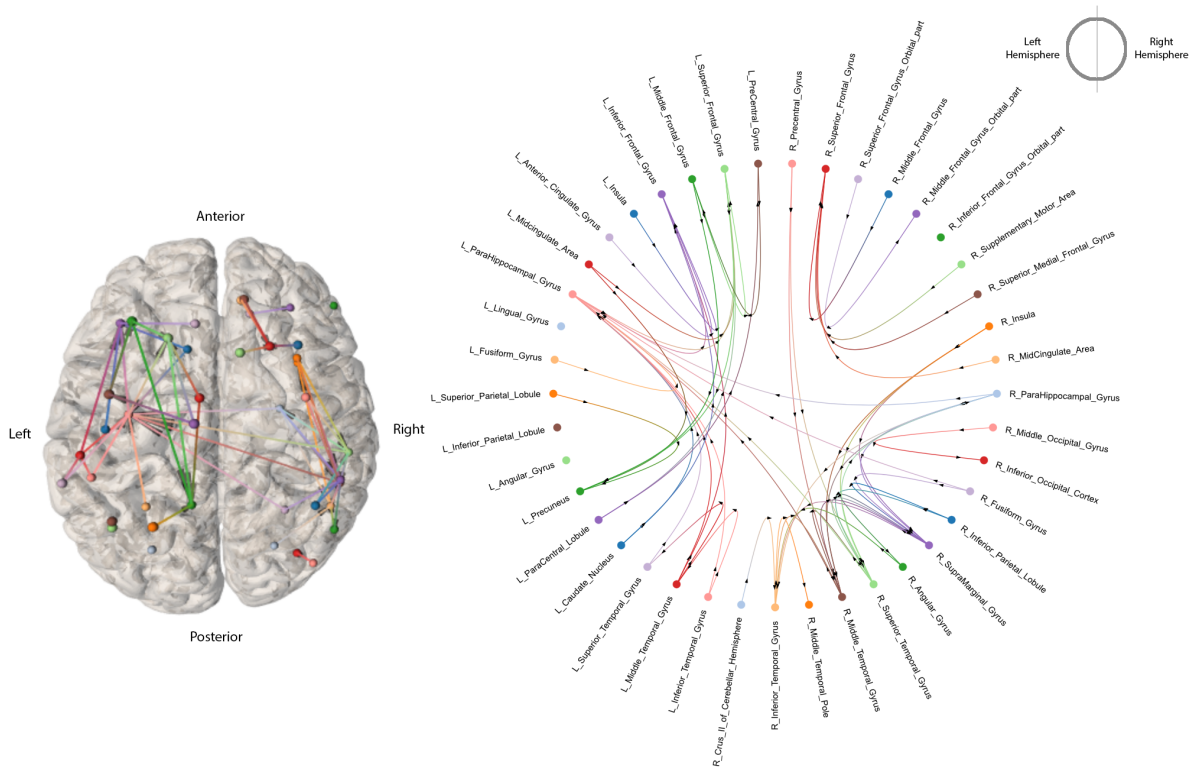

Figure 3.6: *High Intensity Stimulation iEEG Connectome for the entire population of subjects (n=18) analysed in our study based on S-PLV values. (Left panel) 3D connectome is represented in a default normalized brain template, in which each node corresponds to an implanted AAL region. Geometrical node location represents the average position of contacts belonging to the same AAL region. (Right panel) this population based connectome is represented in a circular graph with nodes placed equidistant to each other. Importantly, neither node location nor edge length inform about the distance between two nodes in the real anatomical space. Nodes signal the average MNI x, y, z coordinates of each implanted AAL regions across participants for a given AAL area. For both graphs, arrows present on the edges signal the estimated direction of activity spreads from a leading/driving site (the one receiving gamma stimulation bursts) towards 'follower' sites.*

As can be observed in both figures 3.5 and 3.6, *High Intensity stimulation connectome* edges remain mainly intra-hemispherical, with only 4 of them linking regions of the right and the left hemisphere. We also observed that the Left Parahippocampal Gyrus is the region most frequently acting as a 'receiver' (hosting 9 out of 11 total inwards links), and the Right Middle Temporal Gyrus, hosting 5 out of 7 links. The highest sender region is the Right Superior Temporal Gyrus, hosting 4 out of 7 outwards links, and the Right Parahippocampal Gyrus, hosting 4 out of 5 outward links. The regions showing the highest node degree (amount of inward links + amount of outward links) are the Left Parahippocampal Gyrus (11), the Right Supramarginal Gyrus (8), the Right Superior Temporal Gyrus and the Right Middle Temporal Gyrus (both with 7). Four regions of the connectome exhibit no signs of connectivity.

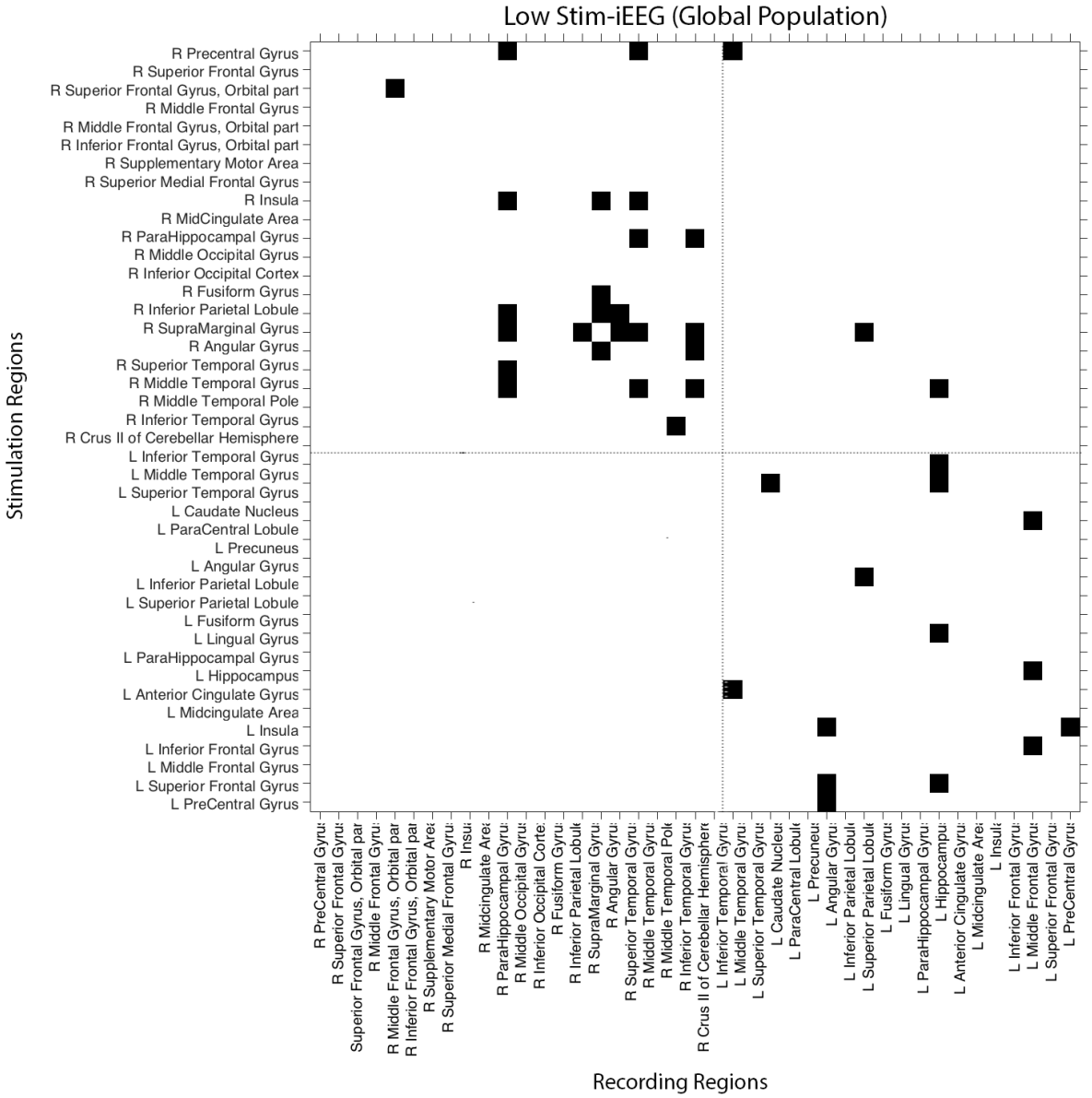

Figure 3.7: *Low Intensity Stimulation iEEG-based Connectome Adjacency Matrix, integrating data for the entire population of patients (n=18) based on S-PLVs. The horizontal and vertical dotted line divide brain regions of the left and the right hemisphere. Each black square represent a pair-wise connection.*

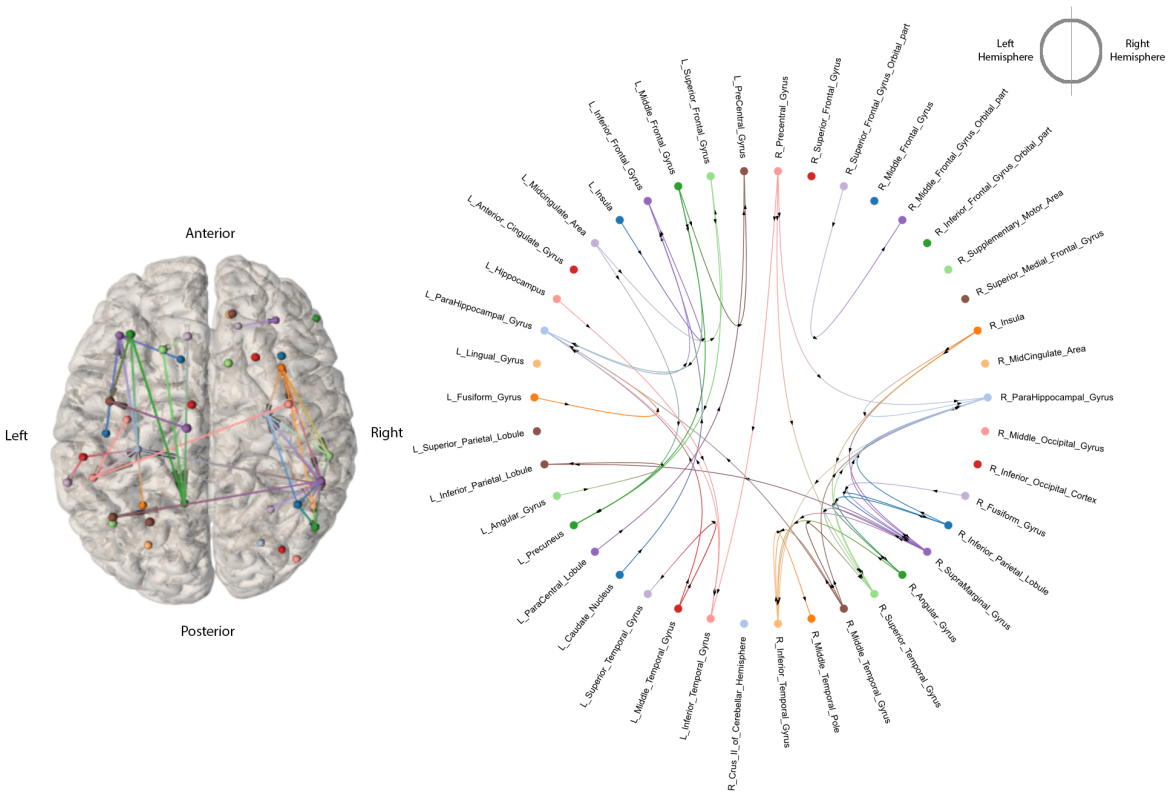

Figure 3.8: *Low Intensity Stimulation iEEG-based connectome, integrating data from the entire population of patients (n=18). (Left panel), 3D connectome represented in a normalized MRI brain template, in which each node corresponds to an implanted AAL region. Node location represents the average x, y, z MNI coordinate position of the contacts belonging to the same AAL region. (Right panel), connectome represented with a circular graph, with standard equidistant nodes (hence non-informative on real intermodal length). Nodes correspond to implanted AAL region hosting at least a multielectrode contact. For both graphs, arrows displayed on the edges represent the estimated direction of the iEEG signal spread driven by the stimulated region onto other brain regions.*

According to *Low Intensity Stimulation iEEG connectome* (see figures 3.7 and 3.8), weak stimulation intensities mainly recruited intra-hemispheric connections. Indeed, a lower number of edges going from the left to the right hemisphere was found (2). Regions with the highest node degree were the Right Supramarginal Gyrus (10), the Right ParaHippocampal Gyrus (8), and Right Superior Temporal Gyrus and Left ParaHippocampal Gyrus (both with 6). The Right Parahippocampal Gyrus was, under such stimulation conditions the region most frequently operating as a receiver, with 6 out of its 8 links conveying inward activity. The highest sender region is the Right Supramarginal Gyrus, with 6 out of its 10 links directing activity outwards. Twelve regions exhibited no signs of subtending pair-wise connectivity.

Finally, a comparison of the *High Intensity Stimulation iEEG Connectome* and the *Low Intensity Stimulation iEEG Connectome* revealed that the number of links present exclusively during the former *High Intensity iEEG-based connectome* (30), observed in figure 3.9, was greater than the number of links recruited only during *Low Intensity iEEG-based connectome* (20), observed in figure 3.10. Also, a comparison of the high intensity and low intensity stimulation iEEG-based connectomes, a significant correlation between non-binarized S-PLVs for both connectomes was found, (rho=0.442, p=0.002).

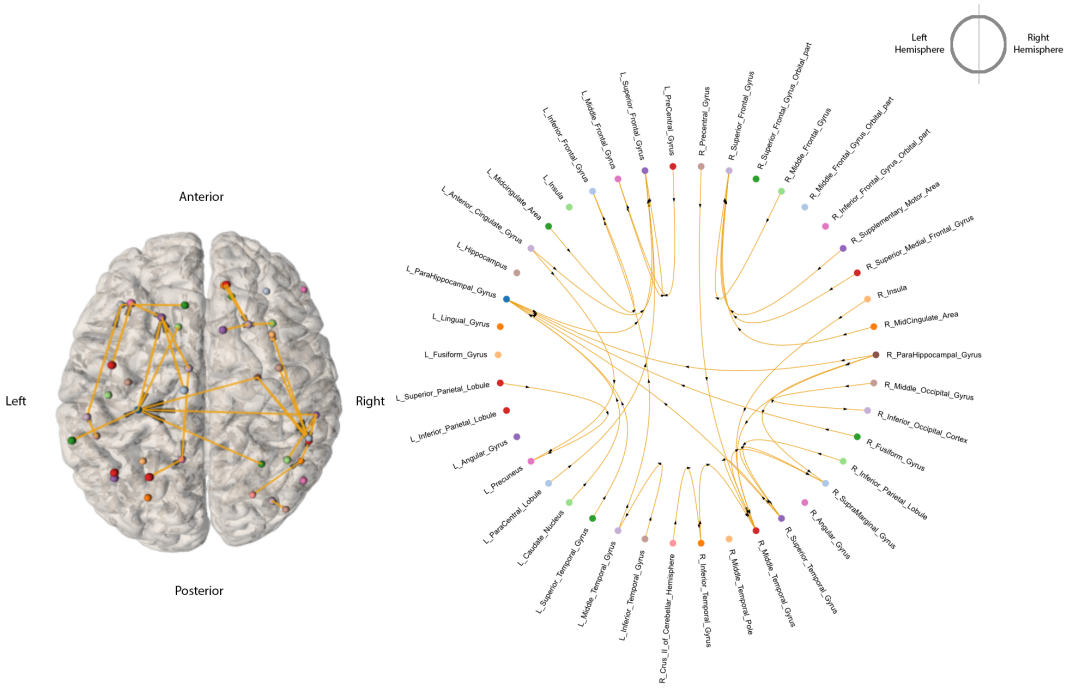

Figure 3.9: *Global connectome of the whole population of studied patients (n=18) showing edges present only during high intensity stimulation-iEEG (in orange).*

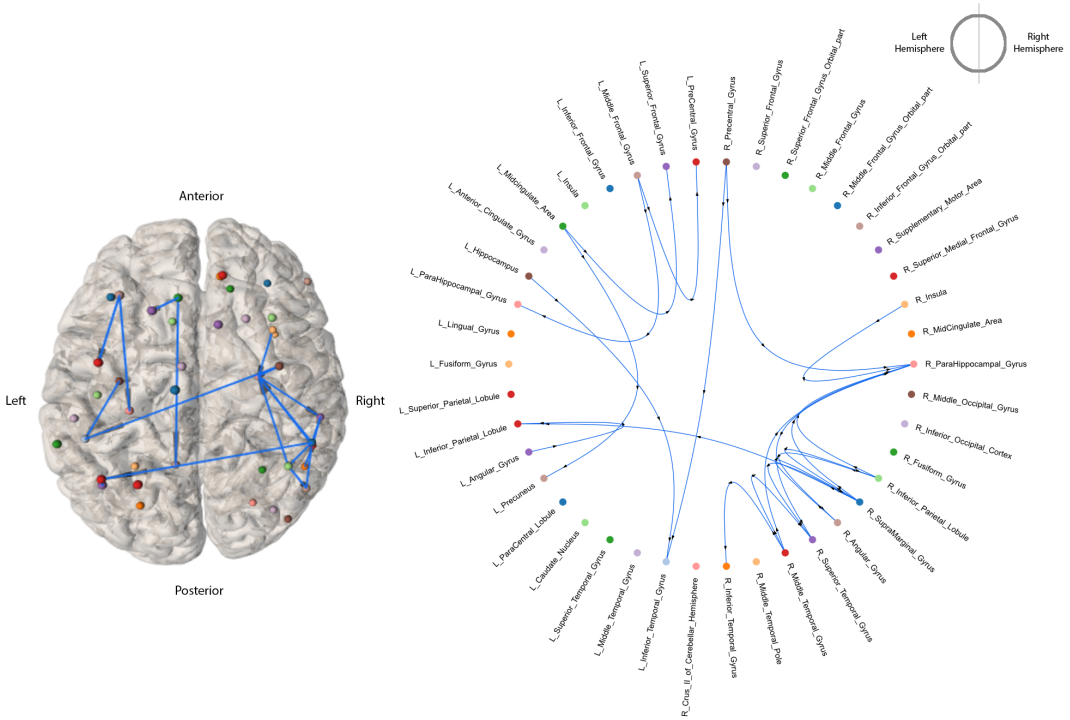

Figure 3.10: *Global connectome integrating data from the entire population of patients included in our study (n=18) displaying the edges present only during low intensity stimulation (in blue).*

3.2 Resting state iEEG-based connectome

As we did for stimulation iEEG-based datasets in the preceding sections (section 3.1), results will first be presented for illustration purposes on the datasets of a representative single patient (n=1, reference number 1998). This will be followed by a presentation of iEEG-based connectome data including the whole population of implanted patients whose datasets were studied in this project (n=18).

3.2.1 Single case connectivity atlas or connectome

The multielectrode implantation scheme for patient ref. 1998 was the same we used to record resting-state (RS-iEEG) and stimulation (Stim-iEEG) datasets (see section 3.1.1). We computed adjacency matrices for both the h^2_{xy} and the mutual information index. Nonetheless, two main reasons advised to put the focus in this section on the former and leave the latter aside: First, both measures showed a high degree of similarity; second, h^2_{xy} provides information about the directionality of information flow which MI is lacking.

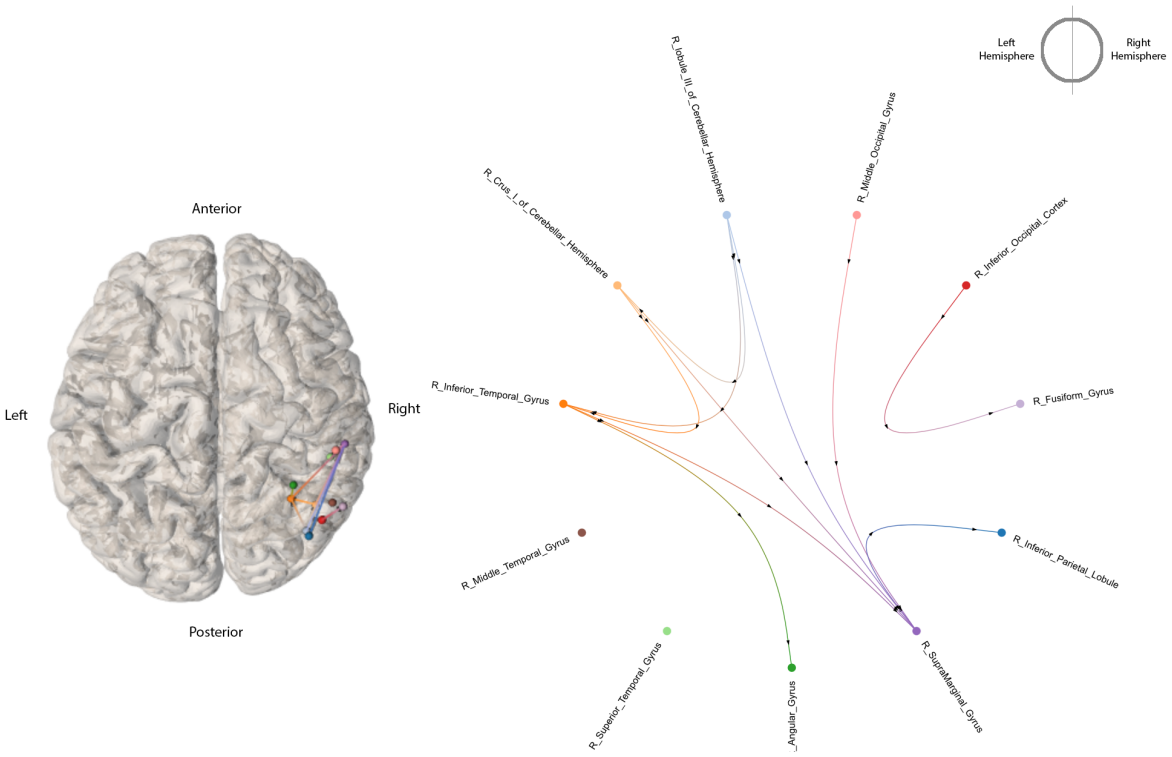

Figure 3.11: *Resting state iEEG-based connectome for patient ref. 1998 (n=1). (Left panel) 3D rendering of the connectome, based for h^2_{xy}, represented on a default and normalized MRI brain template, in which each nodes corresponds to the location of at least a contact implanted on an AAL region. Nodes are located on the average of x, y, z MNI coordinates of the different contacts that are hosted in the same AAL region. (Right panel), h^2_{xy} iEEG based resting state connectome represented on a circular graph in which nodes are depicted equidistantly. In both version of the graph (right and left), arrows depicted on the edges represent the estimated direction of the spread of the signal according to the value taken by the h^2_{xy}.*

As shown in figure 3.11, representing the *Resting-state iEEG-based connectome*, the Right

Supramarginal Gyrus is the area showing the highest node degree (4 inward links and 1 outward link). This region has also the highest inwards node degree. The Right Lobule III of Cerebellar Hemisphere displays the highest outwards node degree, (3 out of 3 links being outwards). Finally, two regions, the Right Middle Temporal Gyrus and the Right Superior Temporal Gyrus, exhibit no connectivity at all, and appear isolated according to our established measures and applied criteria.

3.2.2 Whole population connectivity atlas or connectome

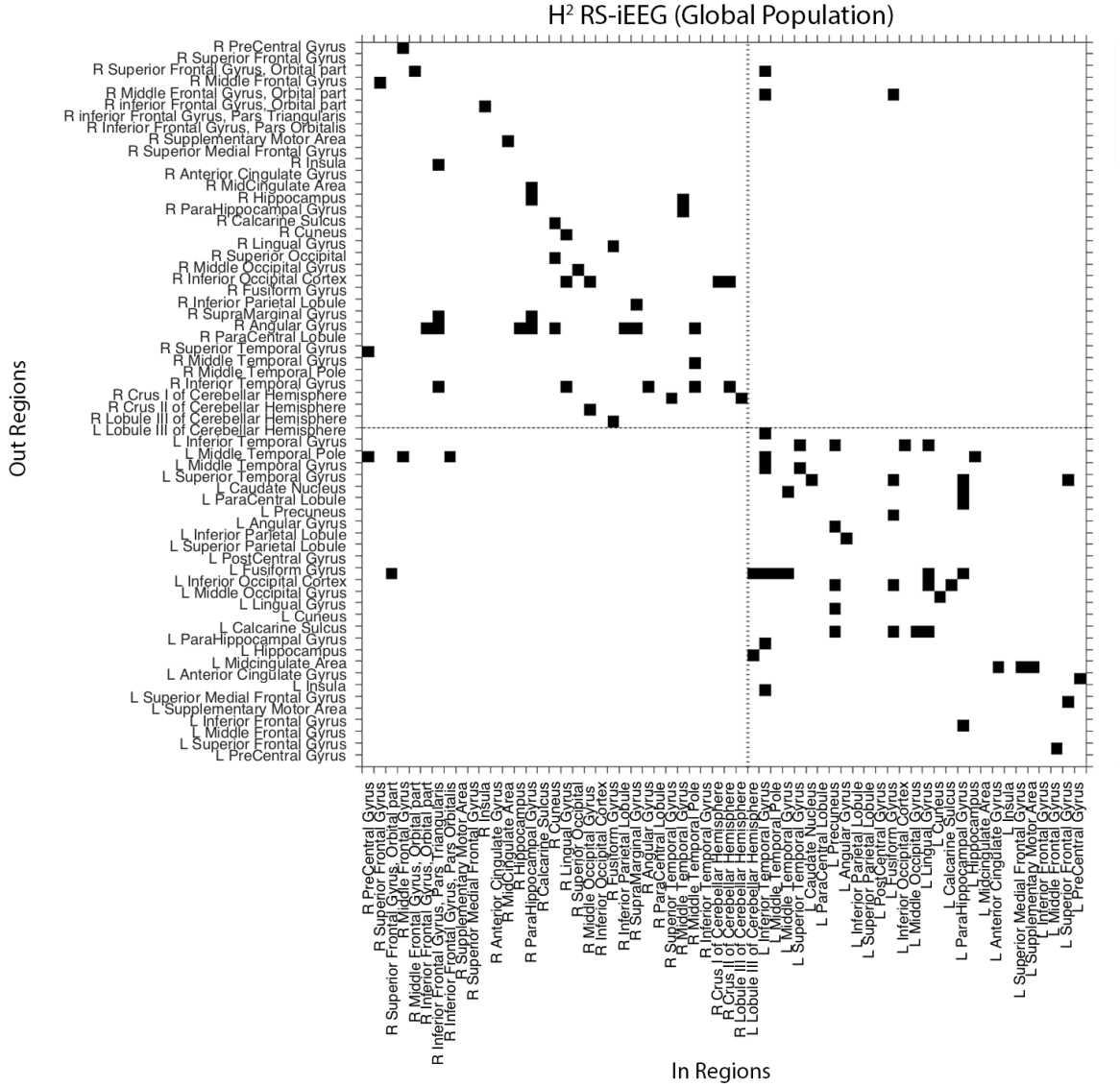

Figure 3.12: *Resting-State iEEG-based connectome matrix, for the entire population of implanted patients (n=18), according to the h^2_{xy} measure. The horizontal and vertical dotted lines divide brain regions from the left and right hemispheres. Cells in black represent pair-wise connections.*

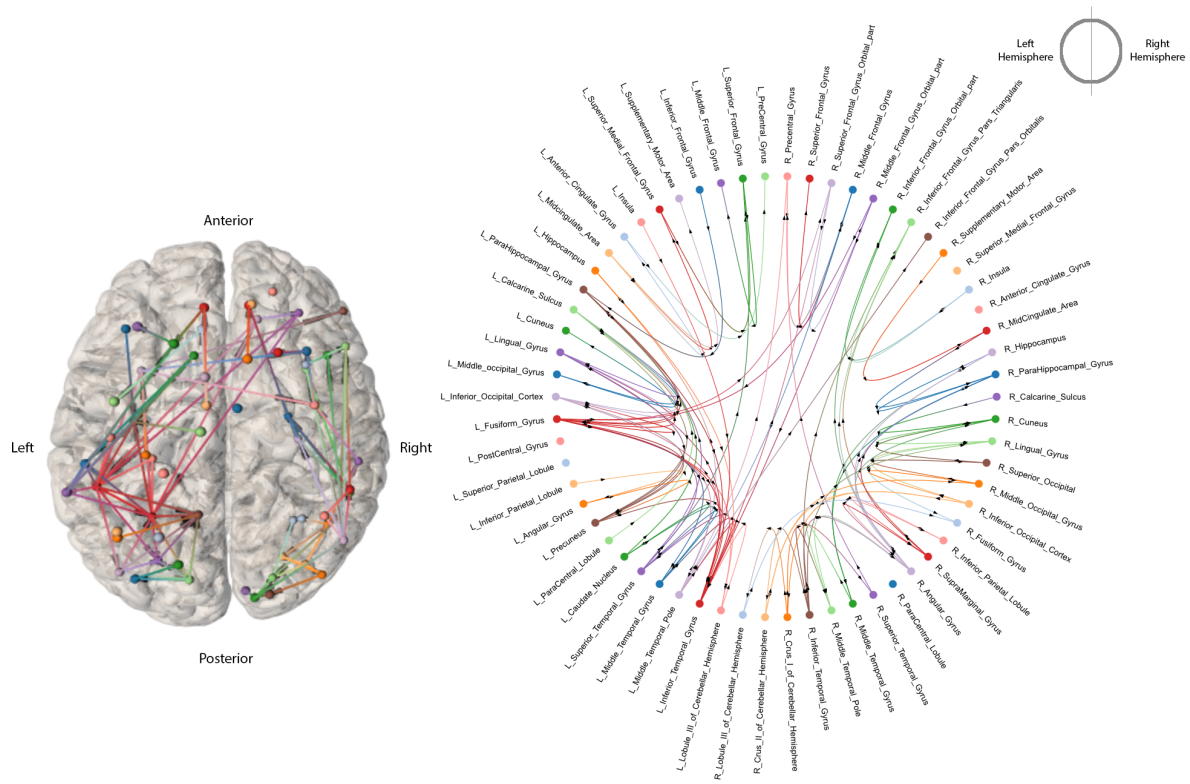

Figure 3.13: *Resting-State iEEG-based connectome, for the entire population of implanted patients (n=18), according to the h^2_{xy} measure. (Left panel) 3D connectomic model represented in a normalized MRI brain template, in which each node corresponds to an implanted AAL regions hosting at least a recording contact. Node location signals the average x, y, z spatial coordinates of contacts hosted by the same AAL region. (Right panel), the connectome is represented on a circular graph made of equidistantly placed nodes, corresponding to each implanted AAL region. In both graphs, arrows displayed on each edge represent the estimated direction of signal flow according to the values revealed by the h^2_{xy} measure.*

As observed in both figures 3.12 and 3.13, for the *Resting-State iEEG-based connectome* calculated according with h^2_{xy} measure, edges showed to be mainly intra-hemispherical, with 5 of them travelling bidirectionally from one hemisphere to the other. The regions with the highest node indegree (hence 'receiver' regions) were the Left Inferior Temporal Gyrus (8) and the Left Precuneus (5). The regions with the highest node outdegree (operating as 'sender' regions) were the Right Angular Gyrus (8) and the Left Fusiform (7). Five different regions exhibited no signs of connectivity.

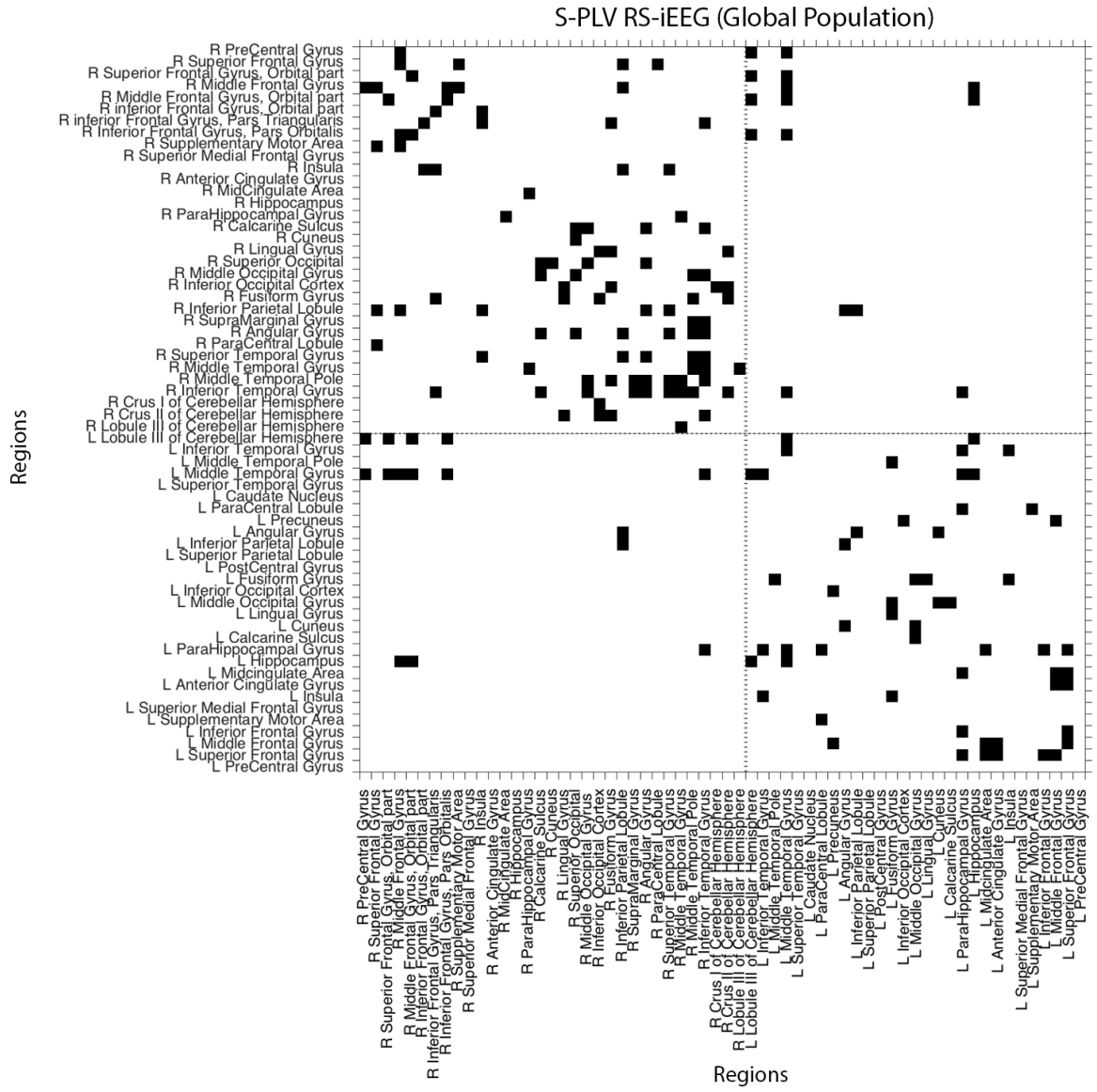

Figure 3.14: *Resting-State iEEG-based connectome calculated with the S-PLV, for the entire population of implanted patients (n=18). The horizontal and vertical dotted lines divide left and right hemisphere brain regions. The black cells display pair-wise connections between nodes.*

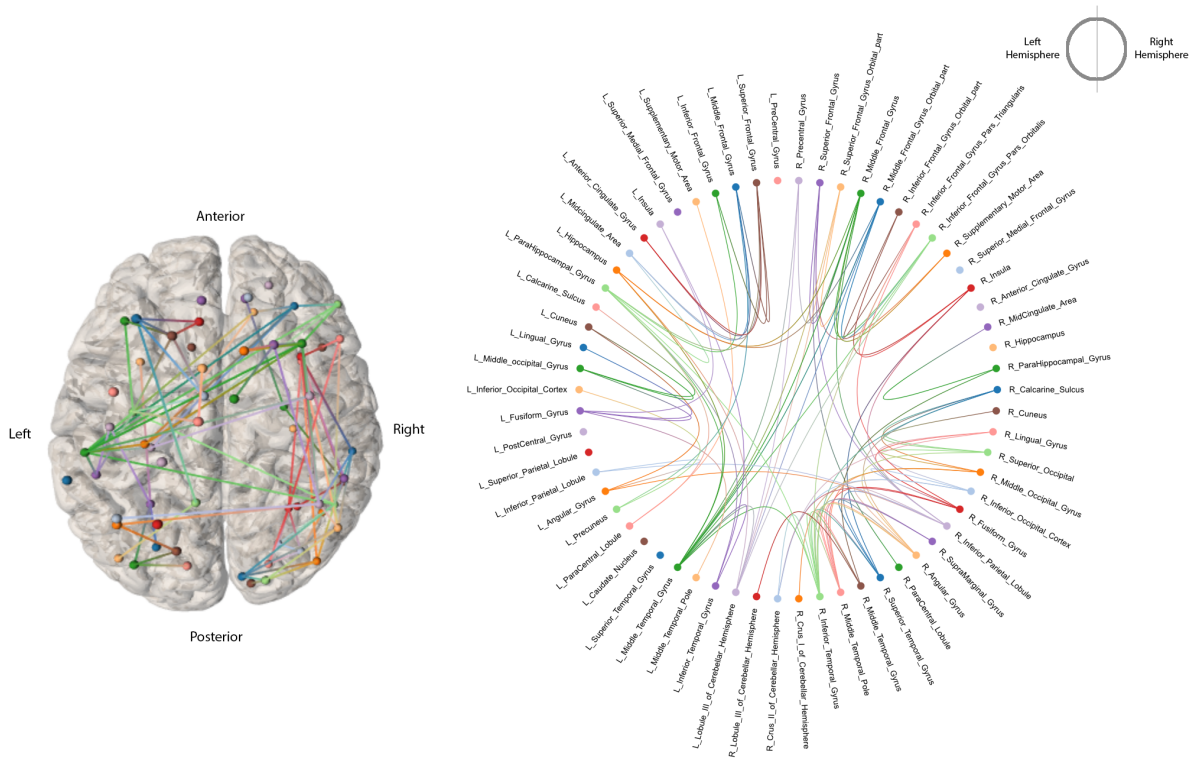

Figure 3.15: *Resting-State iEEG-based connectome, for the entire population of patients dataset (n=18) based on S-PLV measures. (Left panel), 3D connectome represented in a normalized MRI brain template, in which each node corresponds to contacts of an implanted AAL region. The location of each node is estimated as the average x, y, z coordinates of any contacts hosted in the same AAL region. (Right panel), connectome represented in a circular graph with equidistantly positioned nodes, corresponding to each implanted AAL region. In both graphs (Left and Right panels), arrows displayed on each edge represent the direction of the activity or the signal spread.*

As observed in both figures 3.14 and 3.15, for the *Resting-State iEEG-based connectome* estimated on the basis of S-PLV values, edges proved mainly intra-hemispherical (11 out of 93 edges linked areas in one hemisphere to the opposite one). Interestingly, in this case the number of inter-hemispherical links was much higher than those determined according to resting state iEEG-based connectome analyses conducted with h^2_{xy}. The regions with the highest node degree were the Right Inferior Temporal Gyrus and the Left Middle Temporal Gyrus (both with 9 edges). Nine different regions exhibited no signs of subtending connectivity with any other node of the connectome.

As shown previously for *High and Low Stimulation iEEG-based connectome* analyses (see section 3.1.2) performed for the entire population (n=18), a comparison between *Resting-State iEEG-based connectomes* compiled either on the basis of the h^2_{xy} or the S-PLV (see figures 3.16 and 3.17) reveals that the number of links present only either on S-PLV-based resting state connectome or h^2_{xy}-based connectomes is very high (60 edges). A comparison between the non-binarized adjacency matrices of S-PLVs and the binarized adjacency matrices of h^2_{xy} during resting-state, reveals the lack of any significant correlation between these two functional connectivity measures during resting state.

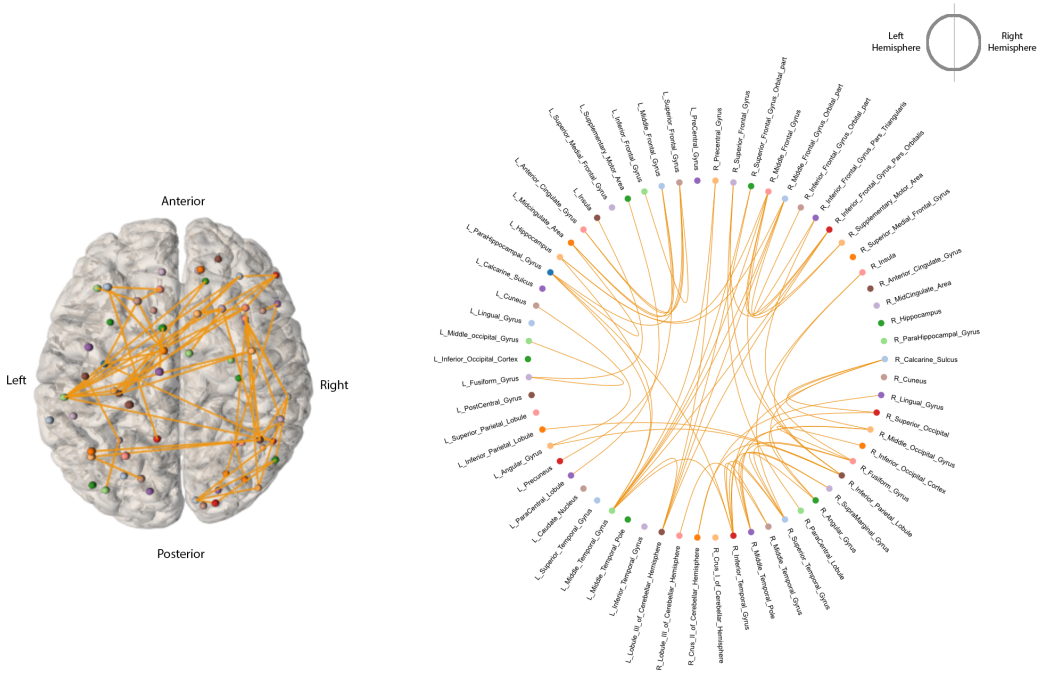

Figure 3.16: *Connectome representation showing edges between nodes present only in the Resting-State iEEG-based connectome using the S-PLV measures (in orange).*

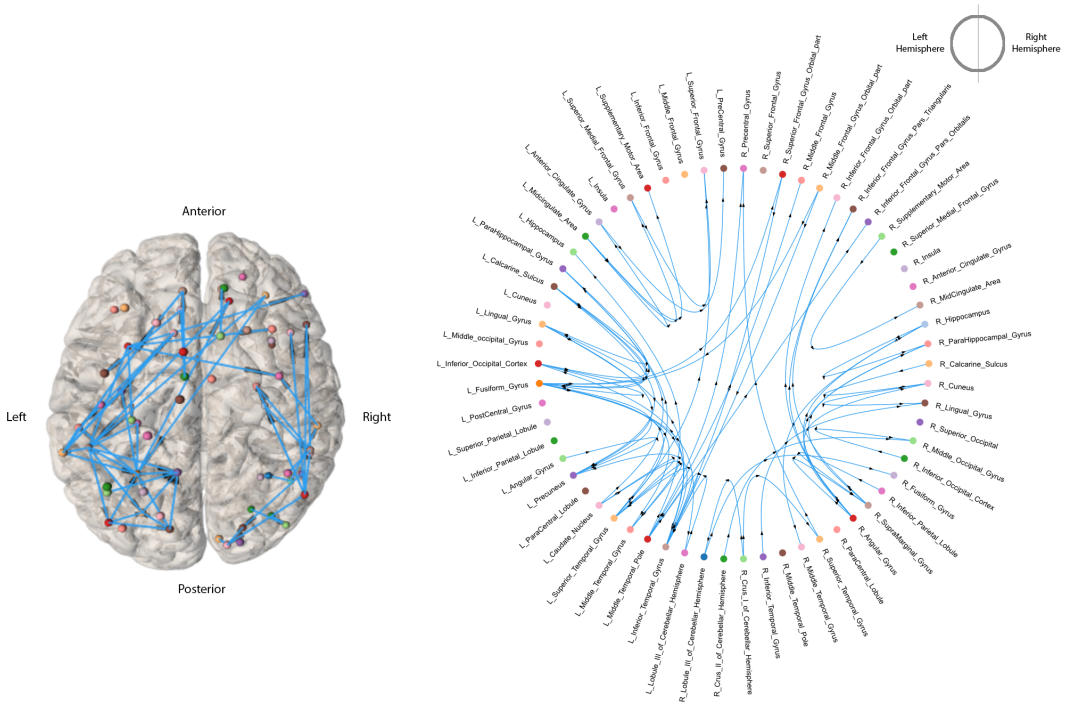

Figure 3.17: *Connectome showing the edges present only during the Resting-State iEEG-based connectome compiled on the basis of the h^2_{xy} measure (in blue).*

3.3 Comparison between resting state and stimulation connectomes

One of the goals of this project was to assess the extent to which the spread of gamma (50 Hz) oscillatory entrainment, induced by local patterns of electrical gamma 50 Hz stimulation across different interconnected brain regions, could be predicted from the *Resting-State iEEG-based connectome*. To this end, we compared both connectomes (*Stimulation iEEG-based connectome* and *Resting-State iEEG-based connectome*). Even though, in contrast with h^2_{xy} estimates, S-PLV measurements extracted from pairs of resting-state iEEG time series do not provide directionality information, we considered *Resting-State S-PLV* iEEG data (figure 3.15) and *High Intensity S-PLV* for the iEEG data under stimulation (figure 3.6), as the most representative connectomes for both states. The *High Intensity Stimulation iEEG-based connectome*, in detriment of its low intensity counterpart, was chosen because of the superior number of specific links or edges across node pairs of the former when compared to the latter.

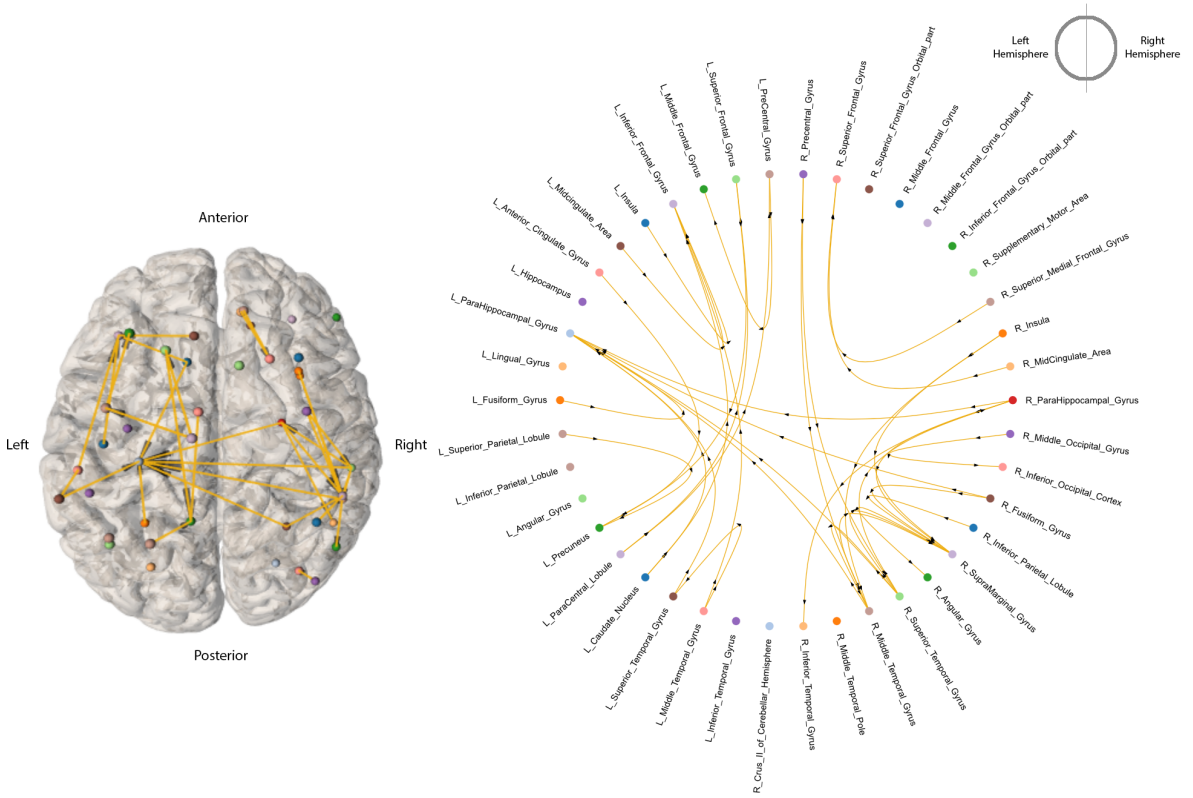

Figure 3.18: *Connectome depictions showing the significant edges or intermodal links present only during gamma 50 Hz electrical stimulation (in orange) for the whole population of implanted patients studied in this work (n=18).*

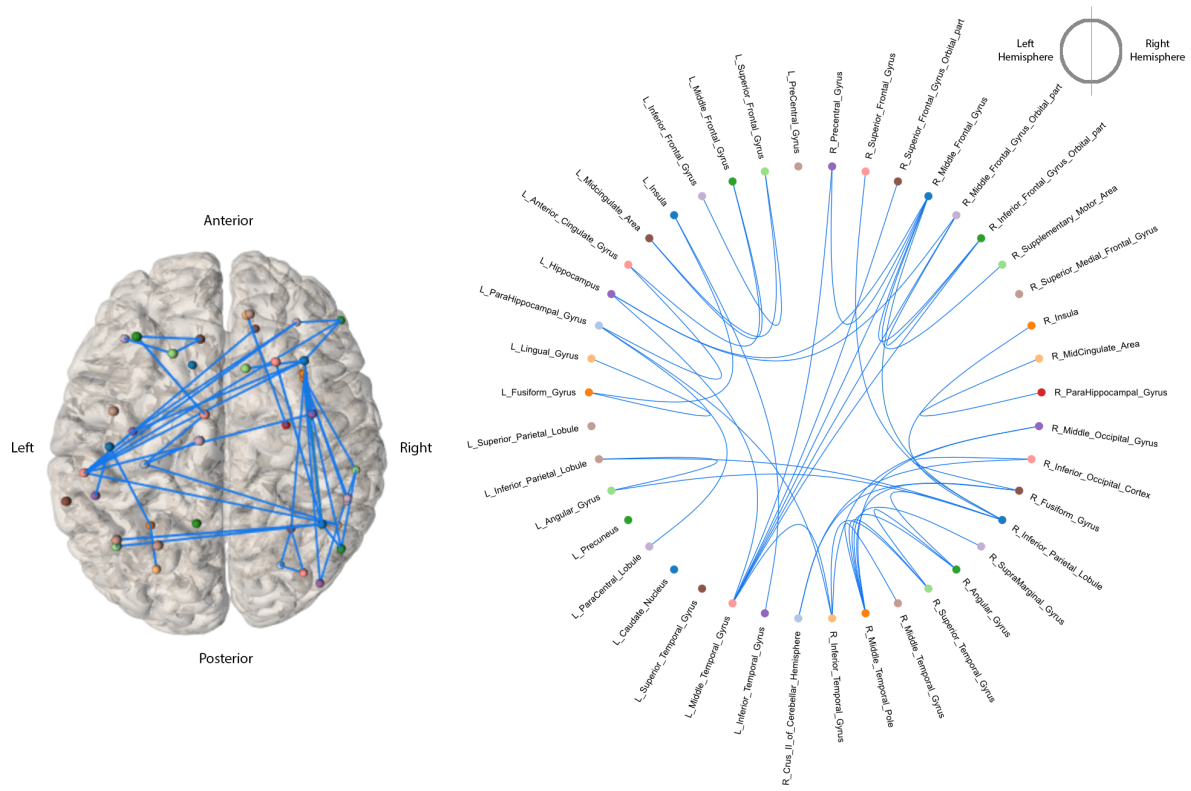

Figure 3.19: *Connectome depictions showing the edges or links present only during resting state interactions measured with iEEG (in blue).*

The number of links specific to each connectome showed similarities: 43 links being present in the *Resting-State iEEG-based connectome* (figure 3.18), but not recruited during *High Intensity Stimulation iEEG-based connectome* (figure 3.19), and 34 in the opposite scenario. This represent 35% of links specific to *Resting-State iEEG-based connectome* intermodal interactions, and 32% derived from *High Intensity Stimulation iEEG-based connectome*.

Moreover, as revealed by figure 3.20a, regions exhibiting higher node degree are often shockingly different across these two main iEEG-based connectomes (resting state vs. electrical stimulation connectomes). In some cases, the strongest nodes in the former connectome, are the weakest in the latter one, or vice-versa. That is the case for the Right Supramarginal Gyrus, which shows a node degree of 8 in the stimulation iEEG-based connectome and only 2 in the resting state iEEG-based connectome; or for the Right Middle Temporal Gyrus, with a node degree of 1 in the former and 7 in the latter. These differences are stated in figure 3.20c, where high positive values or low negative values denote nodes/regions where the discrepancy between node degree when comparing the two connectomes (Stim-iEEG vs RS-iEEG) is high. In contrast, figure 3.20b shows regions for which node degree distributions for both connectomes are similar and increase according to a power law.

Overall, at difference with *High* vs. *Low Stimulation Intensity iEEG-based connectomes* (which were significantly correlated), we could only find a trend towards a correlation across S-PLVs for resting state-iEEG and the stimulation-iEEG connectomes, performed prior to thresholding adjacency matrices (rho=0.188, p =0.053 (Spearman) suggesting that *Resting-State iEEG-based connectome* incompletely predicts the structure of the gamma 50 Hz stimulation connectome or vice-versa.

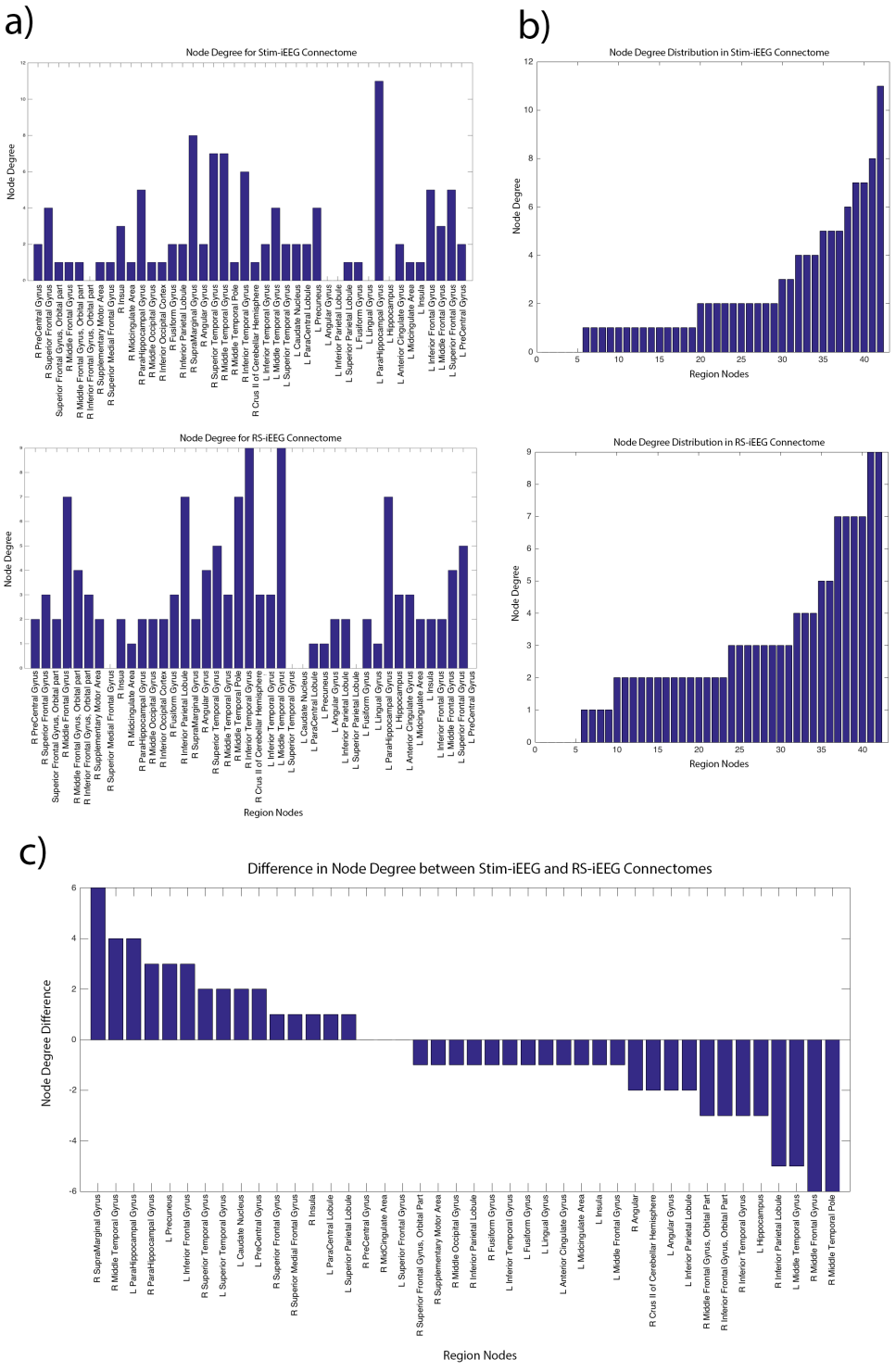

Figure 3.20: *Histogram of Node Degree values comparing data from the stimulation iEEG-based connectome and the resting state iEEG-based connectome. (Panel A, top left) shows node degree for both connectomes, with the higher bars indicating higher node degree for the node. (Panel B, top right) displays node degree distribution data, from the lowest to highest node degree levels. (Panel C, bottom row) shows the difference in node degree between the two types of connectomes (Stim-iEEG and RS-iEEG), in descending order. Positive values signal brain areas for which the node degree is higher on stimulation iEEG-based connectome than on the resting state iEEG-based connectome, whereas negative values signal the opposite.*

Chapter 4

Discussion

In this project, we processed iEEG datasets recorded in the context of clinically-guided causal mapping sessions performed in human epilepsy patients implanted intracranially with multi-electrodes, either at rest (resting state iEEG datasets, RS-iEEG) or under the influence of 5 seconds'-long 50 Hz electrical stimulation bursts (stimulation iEEG datasets, Stim-iEEG), delivered focally through pairs of adjacent microelectrode contacts, at either high or at low intensity. We aimed to use such signals to characterize the patterns of functional interactions operating in these two states in the human brain and compare them across to find out if connectivity patterns inferred causally from focal stimulation, could be predicted from resting state functional interaction maps.

We developed a successful sequence of procedures that allowed us to compute, and depict visually, the connectomes subtending functional interactions at the single case or individual patient level (each one with its own implantation scheme), to latter integrate them in a larger atlas integrating datasets from n=18 patients, better extending brain coverage. Several measures informing on the distribution of iEEG signals across brain networks were considered (information transfer index, h^2_{xy}, SPLV) and probed (h^2_{xy}, S-PLV), with the most adapted to each of the two conditions tested (h^2_{xy} for resting state and SPLV- for stimulation datasets) being chosen. A single final common measure, S-PLV, was used to compare to the best of our abilities and, in spite of some standing differences, our resting state and stimulation connectomes in the same population of patients. The data we produced in this project indicated that the architecture (number, nature and, when probed, the directionality of internodal links) of such connectomes proved highly sensitive to the conditions in which such were recruited or probed. Indeed, substantial differences were found between the resting state iEEG-based connectome and the stimulation iEEG-based connectome recruited by 50 Hz stimulation, which was poorly predicted by the structure of the former on the basis of estimated S-PLV values. Some relevant qualitative and quantitative differences were also found between the high and low stimulation connectomes with regards to specific intermodal links. Nonetheless, correlational analyses performed between unthresholded S-PLV values of the former yielded significant results.

We conclude that iEEG data obtained from implanted patients either at resting-state or under stimulation with frequency specific bursts, can be used to characterize with a high level of anatomical accuracy, functional interactions in the human brain and add causal value of correlational inferences. A connectome representative of the human brain will require, however, the integration in a common anatomical space of datasets from a large population of participants, as to overcome regional sampling biases (i.e., sampling concentrated in specific brain regions that are most likely the source of seizures, hence more likely to be implanted and monitored at the expense of cortical regions from which we rarely have iEEG datasets). More specifically, our data suggests that the architecture of a connectome entailing the same nodes (i.e., based on either resting-state or stimulation-evoked iEEG data from the same nodes or brain areas), hence likely subtended by the same anatomical networks, are highly sensitive to the recording conditions and procedures with which these are probed or recruited, hence highly state and method dependent.

Most importantly and, in spite of potential methodological weaknesses discussed further in upcoming paragraphs and the need for larger samples of iEEG datasets, our data suggests that causal connectomes elicited via focal stimulation (in our case by 50 Hz gamma patterns) can only be poorly predicted by resting-state connectivity operating on the same network. We conclude,

that while the underlying structural networks (defined white matter connectivity patterns, so called structural connectome) allowing flow of activity and signals remains the same, the patterns of functional interactions subtended by anatomical connections can be multiplexed, hence may take different "architectures" (organization, extent, efficacy levels, degrees etc.) as a function of the type (frequency, amplitude, phase-locking level) and nature (physiological or artificial) of the activity flowing into and through the system. As a result, taking structural connectivity patterns as the unique solid basis, human brain functional connectome mapping effort cannot be only based on the data generated by a single correlation technique (resting fMRI, MEG or EEG) or causal approach (single pulse stimulation and evoked potentials) but must causally probe and define its flexible architecture for different types of spatio-temporal coding signals (at different frequencies).

Our study adds a new knowledge to the existing panorama regarding connectivity and causality in the human brain, consisting on the comparison of connectomes obtained from resting-state iEEG datasets and the impact of gamma 50 Hz rhythmic patterns produced by electrical stimulation. The latter was evaluated via neural entrainment, conceptualized as the progressive synchronization in time of local oscillators (i.e., circuits of neurons with the potential to fire synchronously) to an external source of energy, such as the intracranial 50 Hz electrical stimulation bursts undertaken in this study.

Previous studies on human brain connectivity have mainly focused on the use of correlation approaches by means of electrocorticography (ECoG), activating superficial layers of the cortex and rarely combined with rhythmic patterns of stimulation adding focal perturbations into brain systems to generate causality[34]. Indeed, at difference with ECoG approaches, the originality of our study and the data we generated thanks to it, were made possible by the use of intracranial electroencephalographic approaches (iEEG), which provides an unbiased exploration of all cortical layers, including III and V, containing pyramidal neurons, the ultimate substrate of excitatory long-range connections[35, 36]. This is because, in contrast with ECOG, intracranial multielectrodes are inserted in depth, instead of remaining on the pial surface of the cortex. Recent connectivity studies have processed iEEG data, but focusing on widespread patterns of functional connectivity under resting-state[37] or exploring the very local electrophysiological impacts on the sites on which stimulation is delivered[38], neglecting a larger network-based hodological perspective. Most importantly, no prior attempt has been made to date to compare in the same population of participants the "architectural" features of a resting state connectome compared to functional connectivity patterns evoked by patterns of stimulation.

To fill this gap, the current project was aimed to assess whether the spread of signals entrained by electrical stimulation depended on stimulation intensity and to what extent these obeyed the same functional paths (functional interactions) already revealed by resting-state recordings. After a detailed qualitative analysis of the global iEEG-based connectomes we defined under stimulation or at resting state, it became clear there were links present in the former (Stim-iEEG connectome) that did not came out in resting state conditions (RS-iEEG). Importantly, this outcome points to the recruitment or activation of additional functional interactions under focal stimulating that might remain "invisible" or "silent" during resting-state recordings, hence that require the use of a focal perturbation to be revealed. Whether these functional interactions are an artificial product generated by an external source of rhythmic gamma stimulation, or they do indeed play a physiological and a cognitive role in normal brain processing, is a key question that we cannot respond on the basis of our data, since it would have required a comparison with the iEEG interactive patterns generated by a task- or behaviour-evoked activity.

Our results allow us however, at least to support the notion that stimulation-iEEG based connectome and the resting state iEEG connectome based on S-PLV values have different architectural properties, and the former cannot be easily predicted by the latter. Indeed, a comparison of S-PLV values (prior to matrix thresholding) from the stimulation iEEG-based (Stim-iEEG)

and the resting state iEEG-based (RS-iEEG) adjacency matrices yielded a non-significant correlation (rho= 0.188, p=0.053) between the two.

Differences were particularly visible in regions such as the Right Supramarginal Gyrus, the Right Middle Temporal Gyrus and the Left Parahippocampal Gyrus, regions with a strong connectivity during stimulation (Stim-iEEG dataset) but almost no links (hence edges of the connectome graph) at resting state (RS-iEEG). Since our stimulation connectome specifically tested the recruitability through the entrainment of extended intermodal interactions responsive to gamma (50 Hz stimulation), these differences could have been caused by the fact the underlying frequencies at which these two regions can generate rhythmic activity, according to their local organization (the so called natural frequency fingerprint), might exclude 50 Hz gamma patterns. Nonetheless, this possibility is unlikely and will require further analyses, since gamma rhythms are omnipresent across cortical regions and, moreover, highly synchronized external sources of electrical stimulation delivered directly to the brain tissue may eventually forcedly entrain the system at the delivered frequency regardless of its natural frequency fingerprint.

Our fair attempt to provide a qualitative (and eventually quantitative) comparison between the stimulation (Stim-iEEG) and resting-state (RS-iEEG) connectomes, compiled in our cohort of n=18 patients, was undertaken using a common measure to estimate functional interactions, such as the S-PLV. Unfortunately, the details on how data were processed to obtain the optimal coupling estimate between pairs of time-series recorded by multielectrode contacts from specific brain areas could not be exactly identical. Indeed, relevant differences preventing fully fair comparability between these two connectomes were caused by the intended use of the state-of-the art, hence most adapted, coupling measures available for each (initially h2 for RS-iEEG and S-PLV for Stim-iEEG, since the former could not be applied to a modelled stimulator output signal). Moreover, comparability could have been compromised by specific procedures inherent to the processing of one, but not the other, iEEG dataset, such as the need for removal and data interpolation of stimulation artifacts (only necessary for the Stim-iEEG but not for RS-iEEG dataset), which was not applied to resting-state signals, to avoid modifying artificially their structure. Similarly, we employed a different data epoching strategy for the resting-state iEEG dataset (in which we averaged 2 seconds' long iEEG epochs to end up with a single 2 seconds time-series (prior to h2 or S-PLV calculations) , when compared to the stimulation iEEG dataset (in which no averaging was carried our prior to S-PLV analyses). Finally, whereas for resting-state dataset, S-PLV values were calculated between pairs of biologically generated iEEG signals, in the stimulation dataset, such parameter was estimated between a biological iEEG signal and a modelled stimulator output function (see Amengual et al. Sci Reports 2017 for details). Therefore, in light of such processing differences that we will try to minimize even further in upcoming studies, any comparison between the resting-state and the stimulation iEEG connectomes, or the weak although non-significant correlation (rho=0.188, p=0.052) between the two adjacency S-PLV matrices, needs to be interpreted very cautiously and a definitive conclusion will require further analyses and larger datasets.

Some additional methodological limitations of our study, inherent to the use of datasets generated during clinically-guided causal mapping sessions in intracranially implanted epilepsy patients, are also worth-discussing. In particular, a large variety of implantation schemes across patients and the low number of stimulation parameters such as burst frequency (50 Hz) and duration (5 seconds) are intrinsic limitations of studying local or network related physiological and cognitive phenomena with such human models. Also important, the low number of iEEG samples per site x stimulation intensity on a given patient (which is restricted to keep mapping sessions within a reasonable duration and avoid an overstimulation of the implanted cerebral tissue), could impact the reproducibility and reliability of some individual iEEG observations prone to sources of variability or electrical noise which cannot be easily cancelled out or consolidated, as it is done with TMS-EEG o TACS-EEG approaches by averaging out reasonable number of

similarly recorded trials. Last but not least, even if only iEEG data from non-epileptogenic foci were included in our analyses, the fact that the iEEG datasets are obtained from patients suffering epilepsy limits the extrapolation of these data to the healthy brain and the extent to which they inform on physiological rather than epilepsy-related pathological processes.

On another level of the data processing, concerns could be also raised with regards to have averaged individual contact's (often single trial) iEEG time series across intensity ranges (when the same site was stimulated several times at increasing intensities) but particularly across different sites within the boundaries of the same region of the AAL atlas used for parcellation.. Nonetheless, since implantation was, at all times, guided clinically (according to scalp EEG or symptoms-based suspicions on which brain areas might be most likely the seizing sources) individual contacts were never implanted in the exact same coordinates within the boundaries of an AAL atlas region. Hence, aggregating multielectrode x, y, z MNI coordinates within AAL regions and consolidating iEEG individual data sets on representative estimates from several patients across through averaging (data sets recorded in the vicinity but not exactly the same site) was a necessary evil to carry out the analyses, which places in a very influential role the nature (parcellation criterion being functional, behavioural, cytoarchitectural or white matter connectivity based) and spatial resolution (number and size of regions) of the parcellation atlas used to aggregate contact locations and iEEG data.

Regardless, the high focality of the iEEG and stimulation procedures carried out in such populations of implanted epilepsy patients and the possibility they provide to explore with high spatial and temporal resolution, high signal-to-noise ratio and much limited uncertainty about stimulated sites and iEEG sources (as compared to tACS, TMS coupled to scalp EEG or MEG), to probe brain connectivity in humans largely overweighs many of these weaknesses and makes it unique, promising and potentially high-yielding.

It is finally also worth-mentioning that the electrical stimulation patterns delivered (to generate the stimulation iEEG-based dataset and connectome) had the same frequency of the line-noise in Europe (50 Hz) and data could not be 50 Hz band-pass filtered (or notch filtered) since this is the central frequency at which gamma stimulation was hypothesized to entrain local synchrony and distribute it across the connectome. Regardless, this coincident frequencies often raises concerns about the possibility that outcomes derive from an interaction with line-noise instead of being genuinely generated via a physiological effect. Nonetheless, our analysis suggests this scenario is rather unlikely (see discussion in Amengual et al Sci Rep 2017). First, the gamma power ([45 55 Hz]) was found to increase significantly during the 5 secs stimulation period, as compared to a contiguously preceding epoch right before the stimulation, used as a baseline to ascertain increase of gamma power. Second, even if one can always find a level of phase-coupling prior to the delivery of the 50 Hz stimulation bursts caused by noise-line, the fact that this measure had to be significantly higher during the stimulation to fulfil our criteria for entrainment (see details in methods section) suggests that such S-PLV modulations could not be solely explained line-noise generated artifacts.

Indeed, the hypothesis was that the highly focal stimulation provided by iEEG stimulation has the potential to impose entrainment within frequencies different from the natural frequencies characterizing a given site. Animal studies using frequency-tuned optogenetic stimulation[39, 40] have previously provided support in favour of this notion. Unfortunately, this study whose data had to stick to the clinical state of the art with regards to the stimulation frequency, could not integrate the use of bursts at frequencies different than 50 Hz (which is considered the stimulation frequency that maximizes the likelihood to induce seizures when delivered onto potentially epileptogenic brain tissue). Nonetheless, it would be interesting to compare the same set of analyses we performed using iEEG data generated under electrical stimulation delivered at a different frequency, and assess how the architecture of the functional connectome is dependent on stimulation frequency. Additionally, any of the iEEG-based connectomes we compiled in

this dissertation should be subtended by a common set of hard-wired white matter connectivity patterns, which can be employed flexibly by neural activity as a function of excitability- or activity state-, task- or features of the input coding patterns to distribute signals across networks.

Unfortunately, although diffusion imaging datasets for at least 9 of the 18 patients of our cohort are available, the anatomical characterization of the underlying structural connections in each patient brain was out of the scope of this master dissertation. Nonetheless, it will be very relevant to introduce the structural connectivity data to this analysis, to address the extent to which functional connectivity patterns can be backed up by specific direct/indirect white matter bundles, and the extent to which interindividual differences in structural connectivity might co-vary with measures of internodal coupling such as S-PLV or h2 either at resting-state or during stimulation. Additionally, further studies might combine intracranial stimulation as done in our approach with specific behavioural paradigms, thus helping explore causality between brain oscillation rhythms and cognition in humans. Further developing this research, particularly in large cohorts of implanted patients, could lead to the compilation of reliable atlases of the human brain structural and functional connectivity, integrating their ability to subtend and convey local and widespread frequency specific synchronization signals across flexible, scalable efficient brain connectomes. Moreover, further deepening our knowledge in such directions holds the potential to improve the way in which invasive or non-invasive approaches to stimulation are used to rehabilitate abnormal oscillatory activity that might characterize a variety of neurological and psychiatric conditions.

Bibliography

[1] Olaf Sporns. *The human Connectome : Linking Structure and Function in the Human Brain*. Elsevier Inc., 2009.

[2] Julià L. Amengual, Marine Vernet, Claude Adam, and Antoni Valero-Cabré. Local entrainment of oscillatory activity induced by direct brain stimulation in humans. *Scientific Reports*, (January):1–19, 2017.

[3] K. J. Friston, C. D. Frith, and R. S.J. Frackowiak. Time-dependent changes in effective connectivity measured with PET. *Human Brain Mapping*, 1(1):69–79, 1993.

[4] Karl J. Friston. Functional and effective connectivity in neuroimaging: A synthesis. *Human Brain Mapping*, 2(1-2):56–78, 1994.

[5] Pedro A. Valdes-Sosa, Alard Roebroeck, Jean Daunizeau, and Karl Friston. Effective connectivity: Influence, causality and biophysical modeling, 2011.

[6] Kimiaki Hashiguchi, Takato Morioka, Fumiaki Yoshida, Yasushi Miyagi, Shinji Nagata, Ayumi Sakata, and Tomio Sasaki. Correlation between scalp-recorded electroencephalographic and electrocorticographic activities during ictal period. *Seizure*, 16(3):238–247, 2007.

[7] N.E. Crone, L. Hao, J. Hart, D. Boatman, R.P. Lesser, R. Irizarry, and B. Gordon. Electrocorticographic gamma activity during word production in spoken and sign language. *Neurology*, 57(11):2045–2053, 2001.

[8] Olivier David, Thomas Blauwblomme, Anne Sophie Job, Stéphan Chabards, Dominique Hoffmann, Lorella Minotti, and Philippe Kahane. Imaging the seizure onset zone with stereo-electroencephalography. *Brain*, 134(10):2898–2911, 2011.

[9] Arkady Pikovsky, Michael Rosenblum, and Jürgen Kurths. Synchronization: A Universal Concept in Nonlinear Sciences. *Cambridge Nonlinear Science Series 12*, page 432, 2003.

[10] Gregor Thut, Domenica Veniero, Vincenzo Romei, Carlo Miniussi, Philippe Schyns, and Joachim Gross. Rhythmic TMS causes local entrainment of natural oscillatory signatures. *Current Biology*, 21(14):1176–1185, 2011.

[11] Antoni Valero-Cabré, Bertram R. Payne, Jarrett Rushmore, Stephen G. Lomber, and Alvaro Pascual-Leone. Impact of repetitive transcranial magnetic stimulation of the parietal cortex on metabolic brain activity: A 14C-2DG tracing study in the cat. *Experimental Brain Research*, 163(1):1–12, 2005.

[12] Robert S Fisher and Ana Luisa Velasco. Electrical brain stimulation for epilepsy. *Nature Publishing Group*, 10(10):261–27059, 2014.

[13] P Kahane, L Tassi, S Francione D Hoffmann, G Lo Russo, and C Munari. Manifestations électrocliniques induites par la stimulation électrique intracérébrale par << chocs >> dans les épilepsies temporales. *Neurophysiol Clin*, pages 305–326, 1993.

[14] P. Kahane, L. Minotti, D. Ho mann, A.L. Benabid, and C. Munari. *In Handbook of Clinical Neurophysiology Vol.3*. 2004.

[15] Cristian Donos, Ioana Mindruta, Jean Ciurea, Mihai Dragos Maliia, and Andrei Barborica. A comparative study of the effects of pulse parameters for intracranial direct electrical stimulation in epilepsy. *Clinical Neurophysiology*, 127(1):91–101, 2016.

[16] C J Keller, C J Honey, P Megevand, L Entz, I Ulbert, and A D Mehta. Mapping human brain networks with cortico-cortical evoked potentials. *Philosophical transactions of the Royal Society of London. Series B, Biological sciences*, 369(1653), 2014.

[17] Ryder P. Gwinn and Dennis D. Spencer. Fighting fire with fire: Brain stimulation for the treatment of epilepsy. *Clinical Neuroscience Research*, 4(1-2):95–105, 2004.

[18] Olivier David, Anne Sophie Job, Luca De Palma, Dominique Hoffmann, Lorella Minotti, and Philippe Kahane. Probabilistic functional tractography of the human cortex. *NeuroImage*, 80:307–317, 2013.

[19] Q. Duan, K. Djidjeli, W.G. Price, and E.H. Twizell. Weighted rational cubic spline interpolation and its application. *Journal of Computational and Applied Mathematics*, 117:121–135, 2000.

[20] Paul L. Nunez and Ramesh Srinivasan. *Electrical Fields of the Brain: The Neurophysics of EEG*. Oxford University Press, 2nd edition, 2006.

[21] N Tzourio-Mazoyer, B Landeau, D Papathanassiou, F Crivello, O Etard, N Delcroix, B Mazoyer, and M Joliot. Automated Anatomical Labeling of Activations in SPM Using a Macroscopic Anatomical Parcellation of the MNI MRI Single-Subject Brain. *Neuroimage*, 15:273–289, 2002.

[22] Ernesto Pereda, Rodrigo Quian Quiroga, and Joydeep Bhattacharya. Nonlinear multivariate analysis of neurophysiological signals. *Progress in Neurobiology*, 77(1-2):1–37, 2005.

[23] Pieter van Mierlo, Margarita Papadopoulou, Evelien Carrette, Paul Boon, Stefaan Vandenberghe, Kristl Vonck, and Daniele Marinazzo. Functional brain connectivity from EEG in epilepsy: Seizure prediction and epileptogenic focus localization. *Progress in Neurobiology*, 121:19–35, 2014.

[24] Lionel Barnett and Anil K. Seth. The MVGC multivariate Granger causality toolbox: A new approach to Granger-causal inference. *Journal of Neuroscience Methods*, 223:50–68, 2014.

[25] F Wendling and F Bartolomei. Modeling EEG signals and interpreting measures of relationship during temporal-lobe seizures: an approach to the study of epileptogenic networks. *Epileptic Disorders*, 3(Spec Issue):s67–s78, 2001.

[26] Fabrizio De Vico Fallani, Vito Latora, and Mario Chavez. A Topological Criterion for Filtering Information in Complex Brain Networks. *PLOS Computational Biology*, 13(1):e1005305, 2017.

[27] Gregor Thut, Philippe G. Schyns, and Joachim Gross. Entrainment of perceptually relevant brain oscillations by non-invasive rhythmic stimulation of the human brain. *Frontiers in Psychology*, 2(JUL):1–10, 2011.

[28] Catherine Tallon-Baudry, Olivier Bertrand, Claude Delpuech, and Jacques Pernier. Oscillatory Gamma-Band (30 – 70 Hz) Activity Induced by a Visual Search Task in Humans. *The Journal of Neuroscience*, 17(2):722–734, 1997.

[29] Josep Marco-Pallarés, Estela Camara, Thomas F Munte, and Antoni Rodríguez-Fornells. Neural Mechanisms Underlying Adaptive Actions after Slips. *Journal of Cognitive Neuroscience*, 20(9):1595–1610, 2008.

[30] M Le Van Quyen, J Foucher, J Lachaux, E Rodriguez, a Lutz, J Martinerie, and F J Varela. Comparison of Hilbert transform and wavelet methods for the analysis of neuronal synchrony. *Journal of neuroscience methods*, 111(2):83–98, 2001.

[31] J P Lachaux, E Rodriguez, J Martinerie, and F J Varela. Measuring Phase Syncrhony in Brain Signals. *Hum. Brain Mapp.*, 8(4):194–208, 1999.

[32] J.-P. Lachaux, E Rodriguez, M Le Van Quyen, A Lutz, J Martinerie, and F J Varela. Studying single-trials of phase-synchronous activity in the brain. *International Journal of Bifurcation and Chaos*, 10(10):2429–2439, 2000.

[33] Juliana Yordanova, Vasil Kolev, Rolf Verleger, Wolfgang Heide, Michael Grumbt, and Martin Schürmann. Synchronization of fronto-parietal beta and theta networks as a signature of visual awareness in neglect. *NeuroImage*, 146(November 2016):341–354, 2017.

[34] László Entz, Emília Tóth, Corey J. Keller, Stephan Bickel, David M. Groppe, Dániel Fabó, Lajos R. Kozák, Loránd Eross, István Ulbert, and Ashesh D. Mehta. Evoked effective connectivity of the human neocortex. *Human Brain Mapping*, 35(12):5736–5753, 2014.

[35] H. S. Meyer, D. Schwarz, V. C. Wimmer, A. C. Schmitt, J. N. D. Kerr, B. Sakmann, and M. Helmstaedter. Inhibitory interneurons in a cortical column form hot zones of inhibition in layers 2 and 5A. *Proceedings of the National Academy of Sciences*, 108(40):16807–16812, 2011.

[36] V.B. Mountcastle. The columnar organization of the cerebral cortex. *Brain*, 120:701–722, 1997.

[37] Gabriele Arnulfo, Jonni Hirvonen, Lino Nobili, Satu Palva, and J. Matias Palva. Phase and amplitude correlations in resting-state activity in human stereotactical EEG recordings. *NeuroImage*, 112:114–127, 2015.

[38] Cristian Donos, Mihai Dragoş Mălîia, Ioana Mîndruţă, Irina Popa, Mirela Ene, Bogdan Bălănescu, Ana Ciurea, and Andrei Barborica. A connectomics approach combining structural and effective connectivity assessed by intracranial electrical stimulation. *NeuroImage*, 132:344–358, 2016.

[39] Toshinobu Kuki, Tomokazu Ohshiro, Shin Ito, Zhi Gang Ji, Yugo Fukazawa, Yoshiya Matsuzaka, Hiromu Yawo, and Hajime Mushiake. Frequency-dependent entrainment of neocortical slow oscillation to repeated optogenetic stimulation in the anesthetized rat. *Neuroscience Research*, 75(1):35–45, 2013.

[40] Jianguang Ni, Thomas Wunderle, Christopher Murphy Lewis, Robert Desimone, Ilka Diester, and Pascal Fries. Gamma-Rhythmic Gain Modulation. *Neuron*, 92(1):240–251, 2016.

Annex

Table 4.1: *Summary table with demographic data (gender and age) of the patients (n=18) included in our analyses, the number of implanted multielectrodes, the total number of contacts and the name of the cerebral regions covered by the implantations on each patient. F: Female; M: Male.*

Patient Code	Gender	Age	Number of Electrodes	Number of Sensors	Implanted Regions		
1785	M	25	10	71	· Right Calcarine sulcus (1)	· Right Fusiform gyrus (5)	· Right Middle Temporal gyrus (13)
					· Right Cuneus (1)	· Right Angular gyrus (6)	· Right Inferior Temporal gyrus (8)
					· Right Lingual gyrus (6)	· Right Middle Occipital gyrus (3)	· Right crus I of cerebellum (3)
					· Right Superior Occipital gyrus (3)	· Right Inferior Occipital gyrus (10)	· No encephalic regions (12)
1817	M	19	12	69	· Right Middle Frontal Gyrus, Orbital Part (1)	· Left Angular gyrus (2)	· Left Middle Temporal gyrus (8)
					· Left Hypoccampus (2)	· Left Precuneus (1)	· Right Middle Temporal gyrus (1)
					· Left Calcarine sulcus (1)	· Left Superior Temporal gyrus (3)	· Left Inferior Temporal gyrus (7)
					· Left Cuneus (1)	· Left Fusiform gyrus (8)	· Left Inferior Occipital gyrus (1)
					· Left Lingual gyrus (2)	· Left Middle Occipital gyrus (7)	· Non encephalic regions (24)
1998	F	31	12	82	· Right Supramarginal Gyrus (5)	· Right Inferior Temporal Gyrus (13)	· Right Lobule III of Cerebellar Hemisphere (2)
					· Right Angular Gyrus (7)	· Right Middle Temporal Gyrus (10)	· Right Crus I of Cerebellar Hemisphere (1)
					· Right Inferior Parietal Lobule (2)	· Right Superior Temporal Gyrus (8)	· Right Inferior Occipital Cortex (3)
					· Right Middle Occipital Gyrus (3)	· Right Fusiform Gyrus (9)	· Non-encephalic regions (19)
2006	F	32	7	50	· Left Inferior Parietal Gyrus (5)	· Right Inferior Parietal Gyrus (7)	· Right Angular Gyrus (7)
					· Left Angural Gyrus (1)	· Right Supramarginal Gyrus (7)	· Non encephalic regions (23)
2033	M	28	12	79	· Left Insula (1)	· Left Middle Temporal gyrus (21)	· Non encephalic regions (7)
					· Left Parahippocampal gyrus (22)	· Left Superior temporal gyrus (20)	
					· Left Fusiform Gyrus (6)	· Left Inferior Temporal gyrus (2)	
2040	M	29	9	54	· Left Precentral Gyrus (4)	· Left Superior Frontal Gyrus (12)	· Left Paracentral Lobule (4)
					· Left Supplementary Motor area (8)	· Left Anterior Cingulate gyrus (2)	· Left Middle Frontal Gyrus (10)
					· Left Medial Frontal Gyrus (5)	· Left Middle cingulate gyrus (4)	· Non encephalic regions (5)
2067	M	19	11	82	· Right Inferior frontal gyrus, pars opercularis (2)	· Right Fusiform Gyrus (6)	· Right Angular gyrus (2)
					· Right Inferior frontal gyrus, pars triangularis (2)	· Right Supramarginal gyrus (5)	· Right Superior Temporal Gyrus (1)
					· Right Insula (2)	· Right Middle Occipital gyrus (1)	· Right Middle Temporal gyrus (7)
					· Right Hippocampus (3)	· Right Middle temporal Pole (2)	· Right Inferior Temporal gyrus (21)
					· Right Parahippocampal gyrus (3)	· Right Inferior Occipital gyrus (2)	· Non encephalic regions (23)
2090	F	22	7	48	· Right Superior Frontal gyrus (14)	· Right midcingulate area (1)	· Right Middle Temporal Gyrus (1)
					· Right Middle Frontal gyrus (13)	· Right Superior Frontal gyrus, medial part (1)	· Non encephalic regions (11)
					· Right Supplementary motor area (5)	· Right Inferior Parietal gyrus (2)	
2135	F	25	9	75	· Right Precentral gyrus (2)	· Left Fusiform Gyrus (4)	· Left Middle Temporal Pole (9)
					· Right Superior Frontal Gyrus, orbital part (1)	· Left Middle Temporal Gyrus (10)	· Left Inferior Temporal (17)
					· Right Middle Frontal gyrus (1)	· Right Inferior Frontal gyrus, orbital part (2)	· Left lobule III of cerebellar hemisphere (1)
					· Right Middle Frontal gyrus, orbital part (2)	· Left Hippocampus (4)	· Non encephalic regions (15)

Table 4.2: *Summary table with demographic data (gender and age) of the patients (n=18) included in our analyses, the number of implanted multielectrodes, the total number of contacts and the name of the cerebral regions covered by the implantations on each patient. F: Female; M: Male.*

2171	F	22	8	56	· Right Superior Frontal Gyrus (13)	· Right Middle Cingulate area (9)	· Right Parahippocampal gyrus (4)
					· Right Middle Frontal Gyrus (17)	· Right anterior Cingulate area (5)	· Non encephalic regions (8)
2206	M	27	8	50	· Left superior frontal gyrus (6)	· Left superior Parietal gyrus (5)	· Left Precuneus (7)
					· Left Middle Frontal gyrus (10)	· Left Parahippocampal gyrus (4)	· Left Paracentral Lobule (4)
					· Left Middle Cingulate area (2)	· Left Postcentral gyrus (3)	· Non encephalic regions (10)
2222	F	25	8	63	· Left Parahippocampal gyrus (27)	· Left Middle Temporal gyrus (5)	· Left Inferior Temporal gyrus (6)
					· Left Fusiform gyrus (3)	· Left Superior temporal gyrus (11)	· Non encephalic regions (11)
2230	M	19	8	60	· Right Precentral gyrus (1)	· Right Supramarginal gyrus (7)	· Right Middle Temporal gyrus (6)
					· Right Insula (3)	· Right Superior Temporal gyrus (19)	· Non encephalic regions (8)
					· Right Parahippocampal gyrus (14)	· Right Inferior Parietal gyrus (2)	
2256	F	18	10	54	· Right Precentral gyrus (7)	· Right Middle Cingulate area (3)	· Right Parahippocampal gyrus (3)
					· Right Superior Frontal gyrus (11)	· Right inferior frontal gyrus, pars triangularis (9)	· Right Paracentral Lobule (1)
					· Right Middle Frontal gyrus (14)	· Right Insula (3)	· Non encephalic regions (3)
2259	M	20	8	62	· Left Superior Frontal gyrus (1)	· Left Parahipocampal gyrus (30)	· Left Middle Temporal gyrus (4)
					· Left Middle Frontal gyrus (2)	· Left Caudate nucleus (2)	· Non encephalic regions (9)
					· Left inferior frontal gyrus,pars triangularis (7)	· Left Anterior Cingulare area (2)	
					· Left Insula (2)	· Left Superior Temporal gyrus (3)	
2270	F	22	7	62	· Left Parahippocampal gyrus (23)	· Left Inferior Temporal gyrus (4)	· Non encephalic regions (11)
					· Left Superior Temporal gyrus (6)	· Left Middle Temporal gyrus (18)	
2306	F	25	6	48	· Left Midle Frontal gyrus (3)	· Left Middle Temporal gyrus (15)	· Left inferior Temporal gyrus (13)
					· Left Parahippocampal gyrus (39)	· Left Superior Temporal gyrus (3)	· Non encephalic regions (8)
2316	F	27	10	74	· Left Middle Temporal (2)	· Right Insula (1)	· Right Middle Temporal (18)
					· Left Parahippocampal gyrus (5)	· Right fusiform (6)	· Right Inferior Temporal (13)
					· Right Parahippocampal gyrus (40)	· Right Superior Temporal (5)	· Non Encephalic regions (4)